Faulting and extension rate over the last 20,000 years in the offshore Whakatane Graben, New Zealand continental shelf

Geoffroy Lamarche,[1] Philip M. Barnes,[1] and Jonathan M. Bull[2]

Received 12 July 2005; revised 5 March 2006; accepted 29 March 2006; published 12 July 2006.

[1] Oblique rifting in the offshore Taupo Volcanic Zone, New Zealand, is expressed in widely distributed active normal faulting in the 20-km-wide Whakatane Graben. Active faults are identified along seafloor scarps and displacements of the post-last glacial transgressive ravinement surface (<20 ka), using a network of seismic reflection data and multibeam bathymetry. The rifting involves basement blocks back-tilted by 12–16°, controlled by large NW dipping faults with intersecting antithetic faults within the 3-km-thick sedimentary sequence. Faults along the graben border parallel the rift axis, while those in the center are moderately oblique to it. We present a novel method to estimate the age of a postglacial surface (7.5–20.5 ka), with consideration to spatially varying subsidence and uplift, and measure fault throw across >400 faults. We derive an extension rate at seismogenic depths (6–10 km) across the graben of 13 ± 6 mm yr^{-1}, by summing surface measurements, assuming an average crustal fault dip of 45 ± 15°, and correcting for the discrepancies between surface and deep crustal extension estimates. Structural and kinematic data implies an extension direction 20° oblique to the rift axis, resulting in up to 4.6 ± 2.1 mm yr^{-1} of dextral motion parallel to the rift axis. The strike-slip motion is accommodated by dip-slip displacements on oblique faults in the center of the graben, and oblique-slip faulting along the rift margins. Pure dip-slip in the graben center represents >50% of the total slip, with the Rangitaiki Fault accommodating 25% of the total extension in the graben. **Citation:** Lamarche, G., P. M. Barnes, and J. M. Bull (2006), Faulting and extension rate over the last 20,000 years in the offshore Whakatane Graben, New Zealand continental shelf, *Tectonics*, *25*, TC4005, doi:10.1029/2005TC001886.

1. Introduction

[2] Understanding the mechanisms of development of continental rifts is important because rift systems are excellent settings for the study of fault growth and interactions, the evolution of sedimentary basins, as well as seismic and volcanic hazards [e.g., *Tron and Brun*, 1991; *Kronberg*, 1991; *Morley et al.*, 1992; *Scott et al.*, 1992; *McClay*, 1996; *McClay and Khalil*, 1998; *Roberts et al.*, 2004]. Many field studies of continental rifts, however, lack a three-dimensional approach. Marine studies, as in Greece and the Woodlark Basin, use two-dimensional seismic reflection profiling while sub-aerial continental rifts as in western United States, Iceland, and East Africa concentrate on surface mapping and paleoseismic investigations. This is somewhat compensated by the fact that the three dimensional geometry and development of rift systems are particularly well suited for analogue modeling [e.g., *McClay and White*, 1995; *Clifton et al.*, 2000].

[3] Continental rifts are typically asymmetric and are usually characterized by a deep, narrow, laterally continuous rift valley, bounded by large-displacement normal faults parallel to the rift axis. In oblique extension settings, the fault population may include structures developed at high angles to the rift axis. Although this has been demonstrated in analogue models [e.g., *McClay and White*, 1995; *Clifton et al.*, 2000], there are very few three-dimensional surveys that enable validation of the findings. In particular, the mechanisms of strain partitioning in oblique rifting settings are still poorly understood. Three-dimensional studies are critical to characterize and quantify the distribution of strain and kinematics of faulting in oblique tectonic settings. Fortunately, rift topography facilitates the accumulation of sediments, thus commonly providing essential stratigraphic markers for evaluating deformation.

[4] The Whakatane Graben, New Zealand (Figure 1), is ideally suited for investigating normal faulting processes in an active continental rift, because (1) the northern part of the rift is located over the shallow continental shelf and can be surveyed using marine geophysical techniques, (2) the rates of deformation and sedimentation are high and of the same order, and the marine sediments provide a high-fidelity record of fault structure and growth behavior, and (3) the actively deforming sediments in the graben are dated by volcanic ash deposits, and contain widespread marine erosion surfaces that can be used as structural markers [*Kohn and Glasby*, 1978; *Wright*, 1990]. Integration of a large set of seismic reflection profiles (multichannel and high resolution), and multibeam bathymetry data from the Bay of Plenty provide an exceptional basis to evaluate the history of faulting in a continental rift on timescales of 10^4 to 10^6 years, and unparalleled three-dimensional structural resolution within the Taupo Volcanic Zone (TVZ) (Figure 1).

[1] National Institute of Water and Atmospheric Research Ltd., Wellington, New Zealand.
[2] National Oceanography Centre Southampton, University of Southampton, Southampton, UK.

0278-7407/06/2005TC001886$12.00

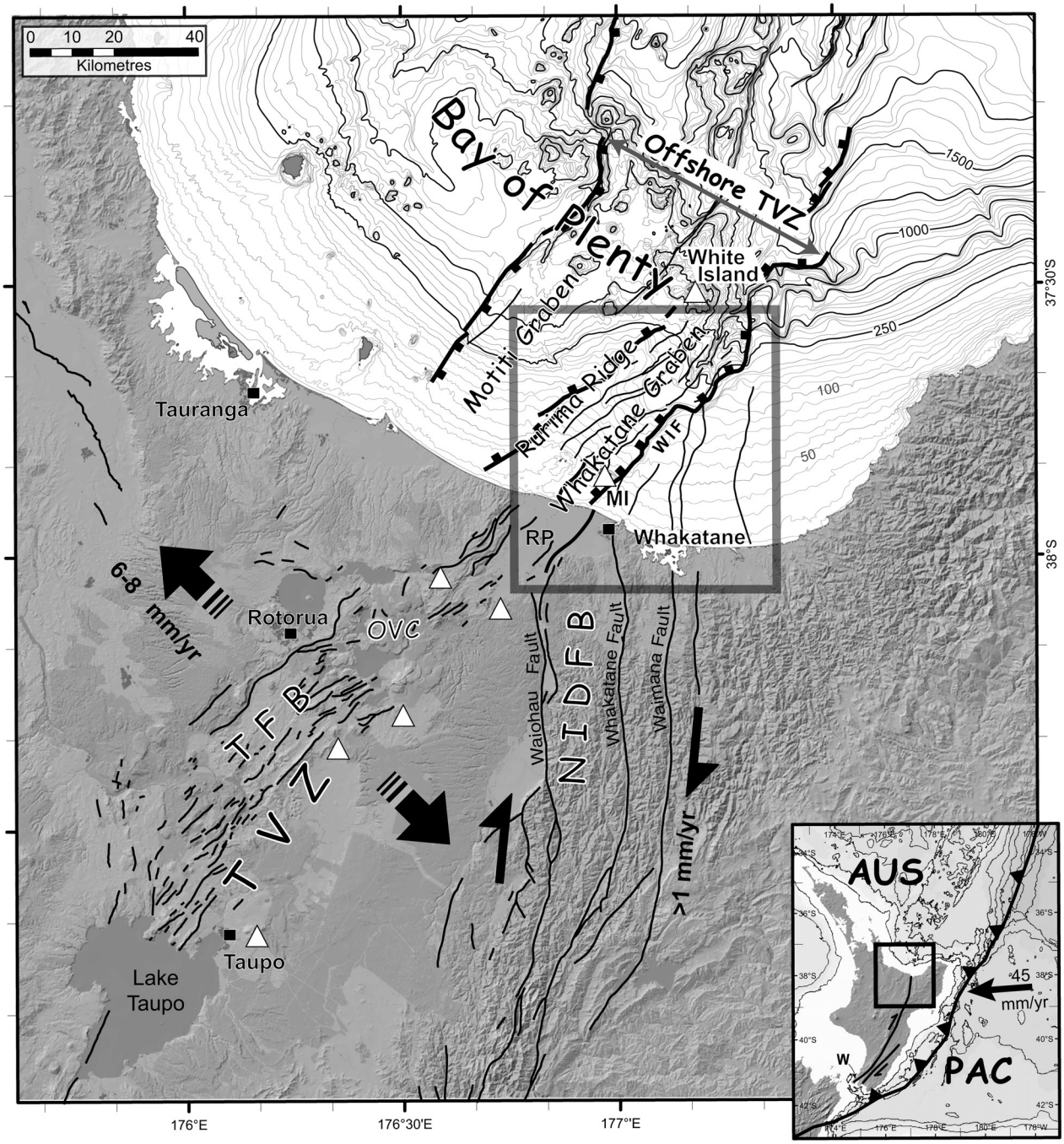

Figure 1. Tectonic map of the Taupo Volcanic Zone (TVZ). Onshore faults from the Taupo Fault Belt (TFB) and the North Island Dextral Fault Belt (NIDFB) are considerably simplified from GNS Science (Lower Hutt, New Zealand) fault database. White triangles indicate active andesite/dacite arc volcanoes. Large black arrows indicate the average extension rate between the margins of the TVZ as determined from *Villamor and Berryman* [2001]. Black half arrows indicate dextral strike slip along the NIDFB; offshore faults are greatly simplified from *Lamarche et al.* [2000]. The main faults bounding the Motiti and Whakatane grabens, in the offshore TVZ, are indicated with thick lines and teeth on the downthrown sides. WIF, White Island Fault. The Whakatane Graben extends southward beneath the Rangitaiki alluvial plain (RP). OVC, Okataina Volcanic Centre; MI, Motuhora Island. Bathymetric contours in meters below sea level. Gray frame indicates the position of Figures 2 and 4. Insert shows geodynamical context of the North Island, New Zealand. W, Wellington; Thick teeth line indicates Pacific-Australia (PAC-AUS) plate boundary along the Hikurangi margin; bold lines with half arrows indicate the NIDFB. NUVEL-1A PAC-AUS plate vector from *DeMets et al.* [1994].

[5] The principal aims of this paper are to document the geometry and slip rates of the late Quaternary (<20 ka) faults within the offshore Whakatane Graben, and present refined estimates of crustal extension rate. In order to evaluate fault slip rates we present a novel method of deriving the age of a widespread late Pleistocene–Holocene diachronous stratigraphic marker. The interpretation of an extensive network of seismic reflection profiles enabled us to produce a significantly revised map of active faults from that of *Wright* [1990], revealing many previously unmapped structures close to urban centers in the coastal Bay of Plenty. The study also provides good constraints on the spatial distribution of extensional strain which allows better understanding of the development and tectonic controls on rift architecture. This paper provides important data concerning the three-dimensional relationships between highly distributed surface faulting and deep-seated displacements on active normal faults. These data have regional importance in terms of improving understanding of the structure of the TVZ, and they provide insights into the structural development and extension mechanisms that likely occur in other continental rifts.

2. Regional Tectonic Setting

[6] The Whakatane Graben is located beneath the continental shelf of the Bay of Plenty, North Island, and extends onshore beneath the Rangitaiki Plains (Figure 1) [*Wright*, 1990; *Nairn and Beanland*, 1989]. Together with the Taupo Fault Belt (TFB) to the south west, the graben is recognized as the principal active rift within the TVZ. The TVZ is a region of Quaternary calc-alkaline volcanism, geothermal activity, intense shallow (<10 km) seismicity [*Bryan et al.*, 1999], and continental extensional faulting within the back-arc environment of the Hikurangi subduction system [*Stern*, 1985; *Wilson et al.*, 1995]. Volcanism commenced in the TVZ about 2 Myr ago [*Houghton et al.*, 1995], and active extensional faulting has been concentrated in the TFB for at least 50,000 yr [*Rowland and Sibson*, 2001; *Villamor and Berryman*, 2001]. Total thinning and stretching of the crust in the TVZ by a factor of ~1.4–2.0 resulted in an average crustal thickness of the quartzo-feldspathic crust of about 16 km [*Stern*, 1985; *Stratford and Stern*, 2004], below which lies a heavily intruded or underplated mafic lower crust [*Harrison and White*, 2004]. The base of the brittle seismogenic zone is estimated at depths of 6–10 km [*Anderson and Webb*, 1989; *Anderson et al.*, 1990; *Bibby et al.*, 1995], with 80% of well-located microearthquakes occurring at depths of <6.5 km [*Bryan et al.*, 1999].

[7] In the offshore Bay of Plenty, the TVZ is a 40 km wide zone of NE trending faulted basement blocks, bathymetric ridges and troughs and volcanic centers that extend to the toe of the continental slope (Figure 1) [*Lewis and Pantin*, 1984; *Wright*, 1992]. On the continental shelf, bathymetric depressions are associated with the Motiti Graben in the west and the Whakatane Graben in the east. The two depressions are separated by the Rurima Ridge, which is underlain by a back-tilted basement block along the western side of the Whakatane Graben [*Davey et al.*, 1995; *Horgan*, 2003]. Numerous late Quaternary faults have been imaged in seismic profiles across the Bay of Plenty, with recent displacements concentrated on Rurima Ridge and the Whakatane Graben [*Wright*, 1990; *Lamarche et al.*, 2000; *Taylor et al.*, 2004, *Bull et al.*, 2006].

[8] Seismic reflection data show that the Whakatane Graben is filled by up to 3 km of sediments, overlying a basement of Mesozoic graywacke with volcanic intrusions [*Davey et al.*, 1995]. Within the graben, active faults displacing the seabed and post last glacial (<20 ka) sediments are densely distributed, with surface traces typically at a spacing of 1–3 km [*Wright*, 1990; *Lamarche et al.*, 2000]. In comparison, thick alluvial deposits obscure the majority of the faults beneath the Rangitaiki Plain [*Nairn and Beanland*, 1989]. *Wright* [1990] used reconnaissance marine 3.5 kHz seismic profiles to determine fault slip rates since 20 ka, and an extension rate across the graben of 3.5 ± 1.7 mm yr^{-1}. This compares with estimates of geodetic extension of ~12 to 15 mm yr^{-1} across the 120 km width of the Bay of Plenty coast [*Walcott*, 1987; *Wallace et al.*, 2004], and 8 ± 2 mm yr^{-1} across the TVZ north of Lake Taupo [*Darby et al.*, 2000]. Late Quaternary subsidence of the continental shelf was estimated to range from 0.4 to 3.5 mm yr^{-1} [*Wright*, 1990], with an average of about 2 mm yr^{-1}. In comparison, *Nairn and Beanland* [1989] estimated subsidence onshore, from borehole data, to be on the order of 1–2 mm yr^{-1} since 0.6 Ma. The present elevations of marine sediments and terraces on the western and eastern margins of the graben indicate rates of uplift of ~1 and 0.5 mm yr^{-1}, respectively.

[9] East of the Whakatane Graben the North Island Dextral Fault Belt (NIDFB) accommodates some 2.5 ± 1 mm yr^{-1} dextral displacement within the graywacke ranges near the Bay of Plenty coast [*Nairn and Beanland*, 1989; *Mouslopoulou et al.*, 2004], and several late Quaternary fault traces extend offshore (Figure 1).

3. Marine Data Sets

[10] The present study is based on a comprehensive set of seismic reflection data, the bulk of which consists of 3.5 kHz and multichannel seismic (MCS) reflection profiles acquired during a survey onboard R/V *Tangaroa* in November 1999 [*Lamarche et al.*, 2000]. The data set is complemented by single channel and 3.5 kHz seismic reflection data acquired in 1988 and 1992 [*Wright*, 1990, 1992], high-resolution seismic reflection data acquired in 2001 onboard R/V *Kaharoa* using uniboom and Chirp sources, and swath bathymetry acquired during two surveys in the northern part of the survey area in 2002 and 2004 (Figure 2). Dredge and core samples complement the geophysical data set and were critical in constraining ages of sedimentary horizons.

[11] Approximately 2200 km of 48-channel seismic reflection profiles were acquired during the 1999 survey. A particular emphasis was placed on the Whakatane Graben with a line spacing of ~3 km. In the center of the graben a 7 × 5 km area was surveyed in a pseudo three-dimensional fashion with a line spacing of 150 m [*Lamarche et al.*, 2000,

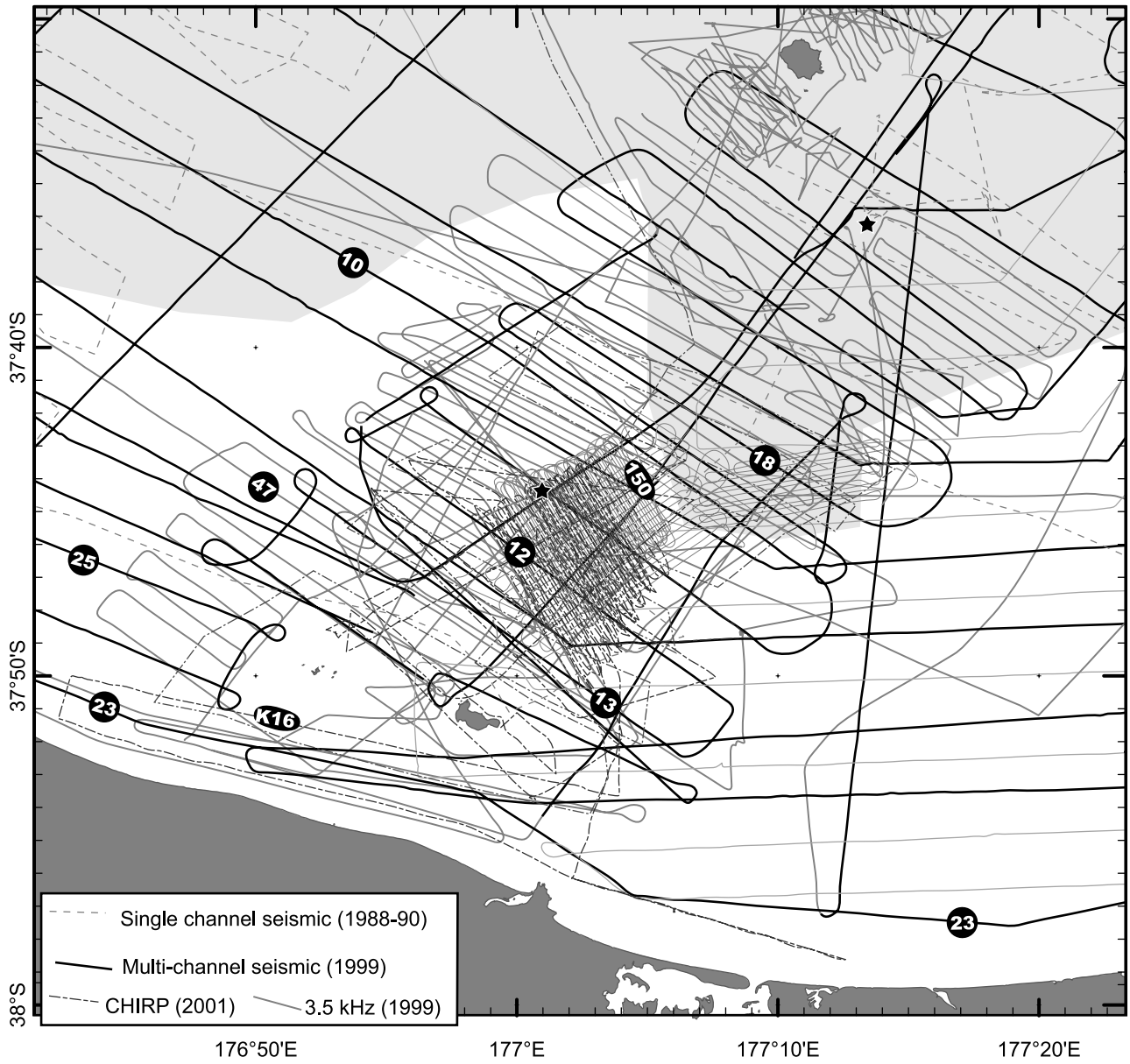

Figure 2. Location of seismic reflection profiles and samples. The very dense number of seismic lines in the center of the survey area emphasizes the pseudo three-dimensional seismic reflection experiment (MCS, Uniboom, 3.5 kHz) undertaken in the center of the Whakatane Graben [*Lamarche et al.*, 2000; *Taylor et al.*, 2004]. Numbers refer to line number of seismic profiles shown in subsequent figures.

Taylor et al., 2004]. The MCS data have a maximum frequency of 150 Hz and provide good resolution down to 2 s (∼2 km, all seismic times are expressed in seconds two way traveltime). The vertical resolution of the MCS is estimated at 3−5 m in the near surface (<∼200 m), and decreases to more than ∼20 m at 2 km beneath the surface. Seismic processing included true amplitude recovery, custom designed band-pass filter and predictive deconvolution functions, long offset mute, normal move out correction, stack and time migration (Kirchoff-Stolt migration). The velocities used for the time migration were derived from stacking velocities and refraction sonobuoy records [*Taylor et al.*, 2004].

[12] More than >5000 km of high-resolution seismic reflection profiles were acquired over the Whakatane Graben. The resolution of geological layers and fault offsets is dependant on the equipment; Uniboom and Chirp data have resolutions of approximately 50 and 20 cm, respectively, while that of the 3.5 kHz is approximately 40 cm. Penetrations of the Uniboom data is 120 m, while that of the Chirp and 3.5 kHz data are 80 m. A band-pass filter was applied to the Uniboom profiles and both the Chirp and

Uniboom profiles were tide and swell corrected. Overall, the typical profile spacing of 1 km outside the pseudo 3D survey area enabled us to confidently correlate faults along strike, and provided excellent coverage of the key stratigraphic markers.

[13] Two swath bathymetry surveys were undertaken in 2001 and 2004 in the northern parts of the Whakatane Graben using a SIMRAD EM300 dual multibeam system. Seafloor topography enabled us to reliably correlate across faults interpreted on seismic reflection profiles.

4. Stratigraphic Framework of the Last 20 kyr

[14] *Wright* [1990] and *Taylor et al.* [2004] documented the stratigraphic sequence deposited in the Whakatane Graben since the last glaciation (<20 ka). Four high-amplitude, laterally continuous horizons (HRS1 to HRS4) have been identified in the high-resolution seismic profiles [*Lamarche et al.*, 2000]. The age of HRS1 (9 ± 1 ka), HRS2 (11.4 ± 1 ka), and HRS3 (13.9 ± 1 ka) were constrained by tephra layers sampled in sediment cores collected in the center of the graben and by extrapolation of sedimentation rate between HRS1 and HRS4 [*Taylor et al.*, 2004]. The age of HRS4 was previously estimated by *Wright* [1990] using the sea level curve of *Carter et al.* [1986], which is based on uncalibrated radiocarbon ages. The most widespread horizon (HRS4) represents the post last glacial transgressive ravinement surface, an extensive erosion surface recognized widely across the New Zealand continental shelf [*Herzer*, 1981; *Carter et al.*, 1986] (Figure 3b). HRS4 formed in very shallow water (probably <20 m) at the low-stand glacial maximum (∼−120 m) and diachronously between the low-stand shoreline and the coast, as the zone of marine abrasion migrated with rising sea level.

[15] Because of its pervasive occurrence in the region, characteristic seismic appearance, and well-understood origin, HRS4 can be used as a key geological marker. For our study it was critical that the diachronous age of its formation be determined, as it directly impacts on the estimation of fault slip rates at any one point. Past studies [e.g., *Lewis and Pantin*, 1984; *Wright*, 1990] did not consider uplift or subsidence since the formation of HRS4. In this study, we present a novel method to estimate the diachronous age of HRS4 by taking into account the vertical rates (VR) of spatially varying uplift and subsidence and considering the observed depth of HRS4 below present-day sea level (D_1) (Figure 3). The corrected time of formation of HRS4 (t_0) can be derived from VR (<0 for subsidence and >0 for uplift), D_1, and the initial depth below sea level at which HRS4 formed (D_0), using

$$D_0 = D_1 + VR\ t_0 \quad (1)$$

[16] The method is best described step by step:

[17] 1. Generate smoothed contours of D_1 from the interpretation of densely spaced high-resolution seismic profiles (Figures 2 and 3a). The smoothing is necessary to avoid local vertical displacement associated with faulting since the last marine transgression.

[18] 2. Generate contours of the estimated rate of post-HRS4 vertical movements, which are superimposed on D_1 (Figure 3a).

[19] 3. Use the postglacial sea level curve for the southwest Pacific region [*Carter et al.*, 1986], which we calibrated to calendar years using the radiocarbon age calibration of *Stuiver et al.* [1998], to correlate the time and the depth of formation of HRS4 (Figure 3c).

[20] 4. Generate tables correlating t_0, D_0, and D_1, using equation (1), for VR varying from +1 to −2 mm yr^{-1}, with increment of 0.5.

[21] 5. At any given location, VR and D_1 are taken from the contour map (Figure 3a) and t_0 is obtained using the correlating tables (Figure 3d).

[22] 6. Finally, we check that t_0 is older than the horizons identified by *Taylor et al.* [2004], HRS1 (9 ± 1 ka), HRS2 (11.4 ± 1 ka) and HRS3 (13.9 ± 1 ka) when HRS4 is imaged beneath these markers.

[23] VR is estimated across the region as follow: The shallow region east of the White Island Fault is attributed an average uplift rate of +0.5 mm yr^{-1}, as determined from uplifted terraces on the coast, east of the township of Whakatane [*Nairn and Beanland*, 1989], and a low-stand paleoshoreline identified in this study at 98 m of water depth ∼30 km north of the coastline (Figure 3a). The age of the paleoshoreline is poorly constrained but assuming it is close to the glacial maximum it corroborates an uplift rate of +0.5 mm yr^{-1} or greater east of the White Island. Rurima Ridge is attributed a maximum uplift rate of +1 mm yr^{-1} along its axis, based on uplifted terraces onshore, west of the Matata Fault (Figure 4), which are uplifting at 0.9–1.7 mm yr^{-1}, and uplifted marine strata 1.3 Myr old on Rurima Islands. The maximum regional subsidence in the center of the graben is estimated at 2 mm yr^{-1} from *Nairn and Beanland* [1989] and *Wright* [1990].

[24] The maximum age for HRS4 is 20.5 ka in the center of the graben where the subsidence rate is at its highest, and immediately to the north of the low-stand glacial maximum shoreline (Figure 3a). The minimum age of HRS4 in the study area is 7.5 ka close to the coast in the center of the graben. Since maximum flooding associated with the last marine transgression, the Rangitaiki Plain and shoreline have prograded seaward up to 10 km [*Nairn and Beanland*, 1989]. The uncertainty associated with the estimation of t_0 is discussed in section 5.1.

5. Methods

5.1. Construction of Fault Maps and Measurements of Displacement

[25] More than 400 traces of faults displacing horizon HRS4 (20–9 ka) were identified on high-resolution seismic reflection profiles, and correlated laterally using multibeam data where available (Figure 2), resulting in the construction of a post last glacial fault map (Figure 4). On the basis of their three-dimensional fault geometry we identified 15 major fault zones in the graben, in which the surface traces merge at depth into one or more,

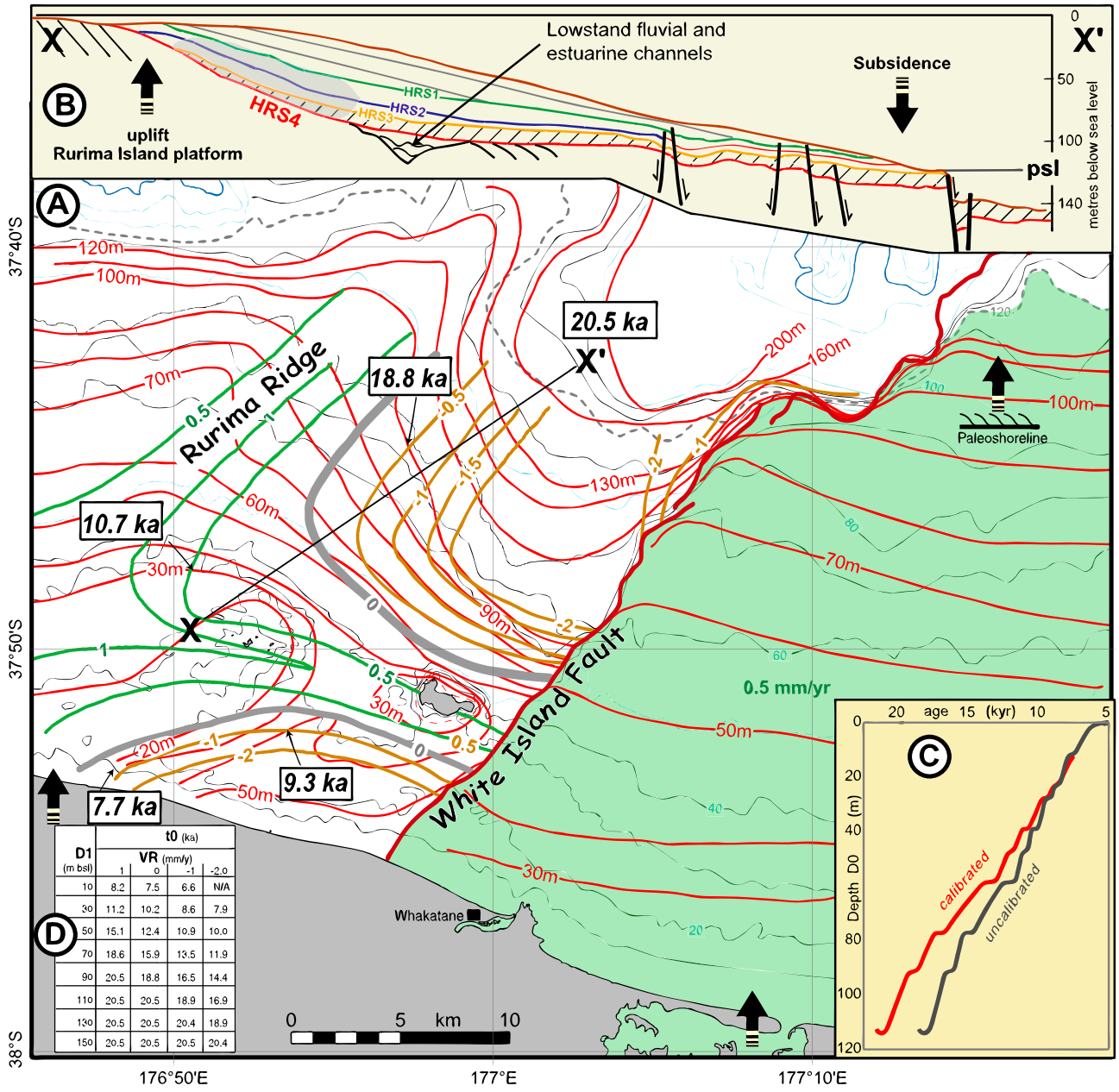

D1 (m bsl)	t0 (ka) VR (mm/y) 1	0	-1	-2.0
10	8.2	7.5	6.6	N/A
30	11.2	10.2	8.6	7.9
50	15.1	12.4	10.9	10.0
70	18.6	15.9	13.5	11.9
90	20.5	18.8	16.5	14.4
110	20.5	20.5	18.9	16.9
130	20.5	20.5	20.4	18.9
150	20.5	20.5	20.5	20.4

Figure 3. Sketch of the method implemented to estimate the diachronous age of HRS4 (t_0). (a) Red contours are the depths in meters below present-day sea level of the top of HRS4 (D_1). These contours are strongly smoothed so to avoid the effect of local fault displacement, and their discontinuity across the WIF reflects the probability that a significant fault scarp existed prior to HRS4. Contours of isovertical movement (VR, in mm yr^{-1}) are in brown for subsidence and green for uplift. Thick gray line indicates no-vertical movement (VR = 0). Green region, east of the White Island Fault, denotes a constant VR = +0.5 mm yr^{-1} rate of uplift. Vertical black arrows show the location where uplift is recognized (uplifted terraces on land and paleoshoreline offshore). The present bathymetry is indicated with light gray contours. Numbers in black frame are examples illustrating the best estimates of time of formation of HRS4 (t_0). (b) Schematic of the postglacial wedge on a strike line up the axis of the Whakatane Graben from Motuhora Island to the outer shelf (position shown as XX′ on A); psl, last glacial maximum paleoshoreline. (c) Calibrated sea level curve of *Carter et al.* [1986] in red (the uncalibrated curve is in black). (d) Age estimates of HRS4 formation (t_0 in ka) from present-day depth below sea level (D_1), for varying rates of vertical movement (VR > 0 for uplift, <0 for subsidence).

closely spaced larger structures (Figure 5). We retain six fault names introduced by *Wright* [1990] (The White Island, Ohiwa, Rangitaiki, Nukuhou, Rurima, and Pukehoko faults), but significantly redefine their structures, and further name seven new fault zones, the South Motuhora, Piripai, Thornton, Moutoki, Tokata, Calypso, and Pokare fault zones. The widespread extent of horizon HRS4, combined with the dense grid of seismic profiles,

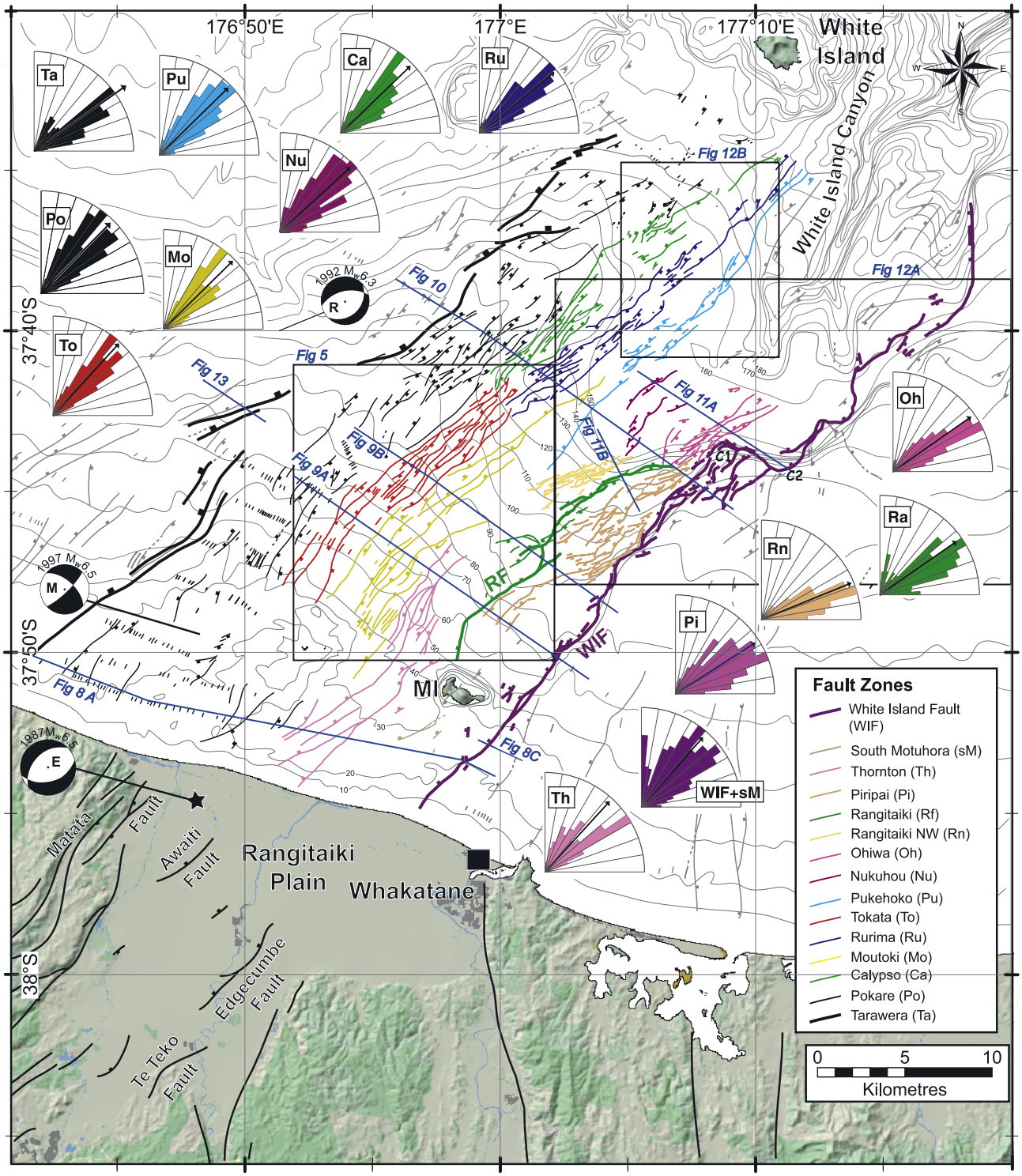

Figure 4

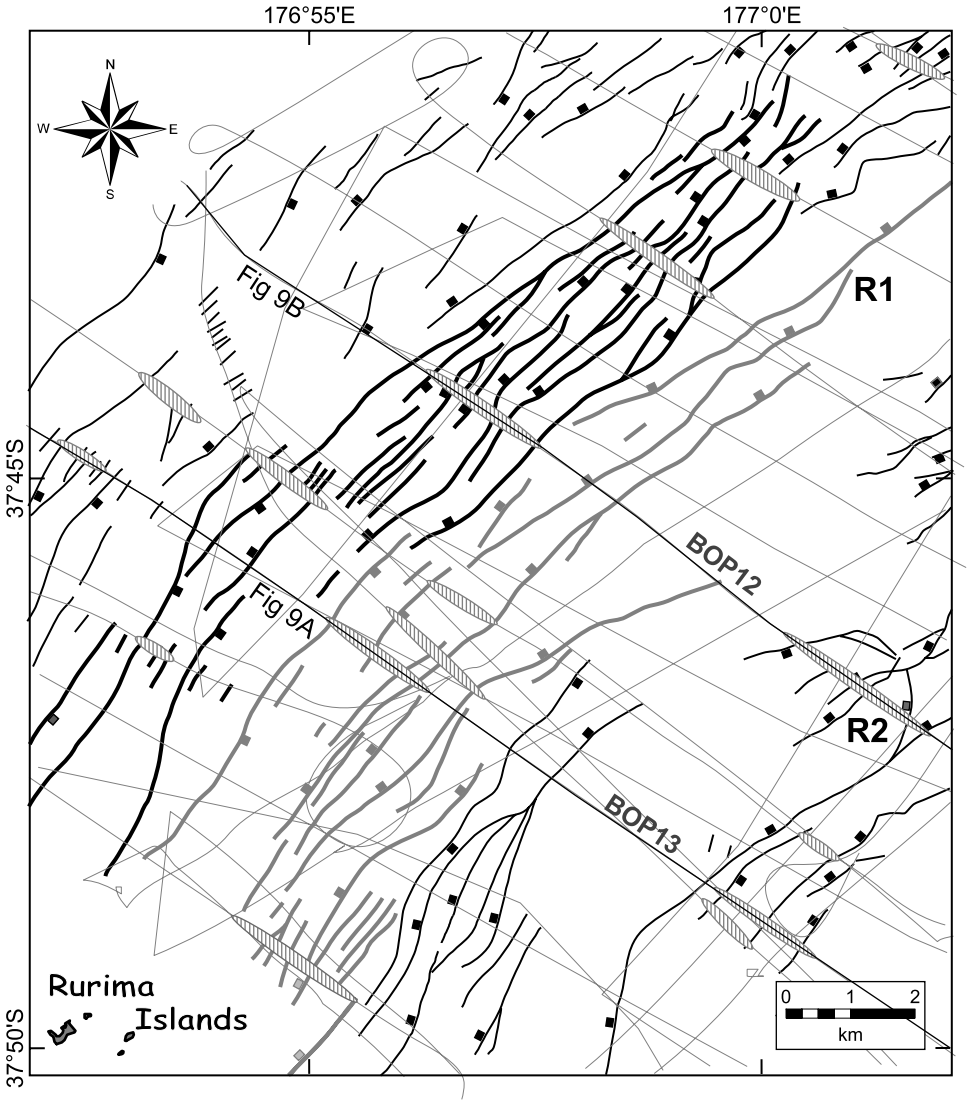

Figure 5. Enlargement of post-20 ka fault map over the southern Moutoki (thick black) and Tokata (thick gray) fault zones. This illustrates the rationale followed for fault group attribution and variations in segment connectivity. Gray striped ellipses indicate faults merging at depth as interpreted on multichannel reflection profiles (thin gray lines), while surface and subsurface fault traces (black lines) are from interpretation of high-resolution seismic data (see Figure 4 for fault group names). R1 and R2 indicate breached relay ramps within the Moutoki and Rangitaiki fault zones.

enabled us to determine the vertical displacement (throw) of this horizon at about 650 locations. We measured the height of seafloor fault scarps and the vertical separation (throw) of HRS4 on high-resolution seismic profiles, by projecting toward the fault the planar segments of the seabed and HRS4 on the footwall and hanging wall, and incorporating where necessary any component of flexure adjacent to the fault in the vertical deformation. The

Figure 4. Post-20 ka fault map of the Whakatane Graben. Faults indicate displacement of HRS4 as identified on high-resolution seismic profiles (Chirp, Uniboom and 3.5 kHz, see Figure 2). Faults are grouped into zones associated at depth from interpretation of multichannel seismic data. Water depth contour is indicated in light gray. Thick lines indicate the graben boundaries. Star on land marks location of the main shock epicenter of the March 1987 M_w 6.5 Edgecumbe earthquake. Locations and focal mechanisms (beach balls) of the Edgecumbe [*Anderson and Webb*, 1989], Matata [*Richardson*, 1989], and Rurima [*Webb and Anderson*, 1998] earthquakes are indicated. C1 and C2 are right angle corners in the surface trace of the White Island Fault (WIF). MI, Motuhora Island. Inserts are fault strike rose diagrams for each fault zone. Rose diagrams are calculated after decimation of every individual fault strands in 50- to 100-m-long segments. Black arrows on rose diagrams indicate the mean direction for each fault zone (Table 1).

Table 1. Post-20 ka Maximum Vertical Separations (Throws), and Vertical Displacement Rates for Fault Zones Identified in the Whakatane Graben[a]

Fault	N	Az	Maximum Throw, m		Age, ka	Maximum Throw Rate		Maximum Dip Slip Rate, mm yr^{-1}		Surface Extension, mm yr^{-1}
			Individual	Cumulative		Individual	Cumulative	Individual	Cumulative	
Eastern Boundary										
WIF	89	41°	42–59	42–59	*17.0*	2.3–3.5		2.0–4.5	2.0–4.5	1.06 ± 0.58
Central Graben										
Nukuhou	19	47°	27	27	20.5	1.32	1.32	1.40 ± 0.35	1.40 ± 0.42	0.48 ± 0.26
Ohiwa	50	55°	26	57	20.5	1.27	2.77	1.35 ± 0.34	2.95 ± 0.88	1.01 ± 0.55
Thornton	46	42°	10.5	19	9.3	0.82	1.76	0.87 ± 0.22	1.87 ± 0.56	0.64 ± 0.35
Rangitaiki NW	190	68°	17.3	38.5	17.5	0.99	2.20	1.05 ± 0.26	2.34 ± 0.7	0.8 ± 0.44
Rangitaiki	494	55°	51.7	60.7	17.5	2.95	3.47	3.14 ± 0.79	3.69 ± 1.11	1.26 ± 0.69
Piripai	270	57°	10.7	19.8	17.5	0.61	1.13	0.65 ± 0.16	1.20 ± 0.36	0.41 ± 0.22
Sth Motuhora[b]	3	60°	3	3.6	9.3	0.32	0.39	0.34 ± 0.09	0.41 ± 0.12	0.14 ± 0.08
Average		55° ± 8								
Rurima Ridge										
Calypso	46	46°	10	27	20.5	0.51	1.32	0.54 ± 0.14	1.40 ± 0.42	0.48 ± 0.26
Rurima	88	51°	22	50	20.5	1.08	2.47	1.15 ± 0.29	2.63 ± 0.79	0.9 ± 0.49
Pukehoko	43	45°	21	34	20.5	1.02	1.70	1.09 ± 0.27	1.81 ± 0.54	0.62 ± 0.34
Moutoki	100	45°	11	24	11.8	0.52	1.54	0.55 ± 0.14	1.64 ± 0.49	0.56 ± 0.31
Tokata	164	42°	7.5	36	11.7	0.38	1.87	0.40 ± 0.1	1.99 ± 0.6	0.68 ± 0.37
Pokare[c]	23	44°	-	28	20.5	-	1.37	-	1.45 ± 0.44	0.5 ± 0.27
Average		46° ± 3								
Western Boundary										
Tarawera	20	54°	11		20.5	0.52		0.55 ± 0.14		0.2 ± 0.11

[a]N is number of measurements along fault strike. The fault average trend (Az) is calculated after decimation of each fault into 50–100 m segment. Maximum individual throw measured within each fault group is indicated. The average trend (Az) and maximum cumulative throw are calculated after 200 m decimation of individual throw profiles (throw versus strike-projected distance) and summation for each group individually. The age of the HRS4 surface, as estimated from this study (see text and Figure 3) is given at the location of the maximum cumulative throw. Error on throw rates is essentially associated with error on HRS4 ages and is estimated to 25% and 30% for individual and cumulative rates, respectively. Dip-slip rates and surface extension are calculated using an average fault dip near the surface of 70°. For the WIF, the range of throw reflects the possibility that the seafloor scarp at this location (16.7 m) may or may not have existed at the time HRS4 formed (17 ka); however, we consider it likely that a surface scarp existed, as indicated on Figure 3.

[b]HRS4 is not constrained south of Motuhora Island, and throw and rate are derived from displacement of HRS1 (9 ka).

[c]Measurements for the Pokare Fault Group are only made along transects T1 to T4 (Figure 14); hence maximum values for individual faults are not available.

vertical separation rate was determined by dividing the throw by the interpreted age of HRS4 (t_0) at each location.

[26] From the many measurements of throws made along strike of each fault zone (Table 1), we construct cumulative vertical displacement profiles from which we derive the maximum cumulative vertical displacements for each fault zone (e.g., Figure 6). Hence we are able to provide the maximum value of vertical displacements, rather than a random value or average, along each identified fault segment (Table 1) and we believe that the derived slip rates represent the maximum contribution of each fault to the cumulated slip rate across the graben.

5.2. Errors in Displacement Measurements and Throw Rates

[27] Errors in the measurements of displacements of HRS4 are derived from uncertainties in horizon pick on analogue profiles, the interval velocities of 1550 ± 25 m s^{-1} [*Taylor et al.*, 2004] used for calculating post-HRS4 sediment thickness, and horizon drag observed on faults. The typical error in determining the depth of HRS4 is 0.8 m. In many cases, the largest cause of error originates from fault drag, which is a local perturbation to the displacement field adjacent to the fault plane, in both the footwall and the hanging wall [*Grasemann et al.*, 2005]. Fault drag is directly associated with displacement along the fault plane and is therefore included in the measurement of fault displacement, using the technique employed by *Chapman and Meneilly* [1991] and *Mansfield and Cartwright* [1996] whereby the planar horizons are projected toward the fault plane. Sediment compaction is considered negligible for the 0–20.5 kyr period [*Taylor*, 2003]. Uncertainties associated with the estimation of fault dip at crustal depth are addressed in detail in section 8.

[28] There are several sources of errors associated with the estimation of the age (t_0) of the HRS4 surface. These include uncertainties associated with (1) the generation of smoothed contours of the depth to the HRS4 horizon (Figure 3); (2) the depth at time of deposition (D_0), i.e., the correlation on the postglacial sea level curve for the southwest Pacific region [*Carter et al.*, 1986], and its recalibration to calendar years, and (3) the estimation of subsidence and uplift (VR). We took a conservative approach in estimating the overall uncertainty on t_0, by making two extreme measurements of D_1, so as to provide a range of results. The two extreme estimates are derived using D_1 ± 5 m on the depth of HRS4, and

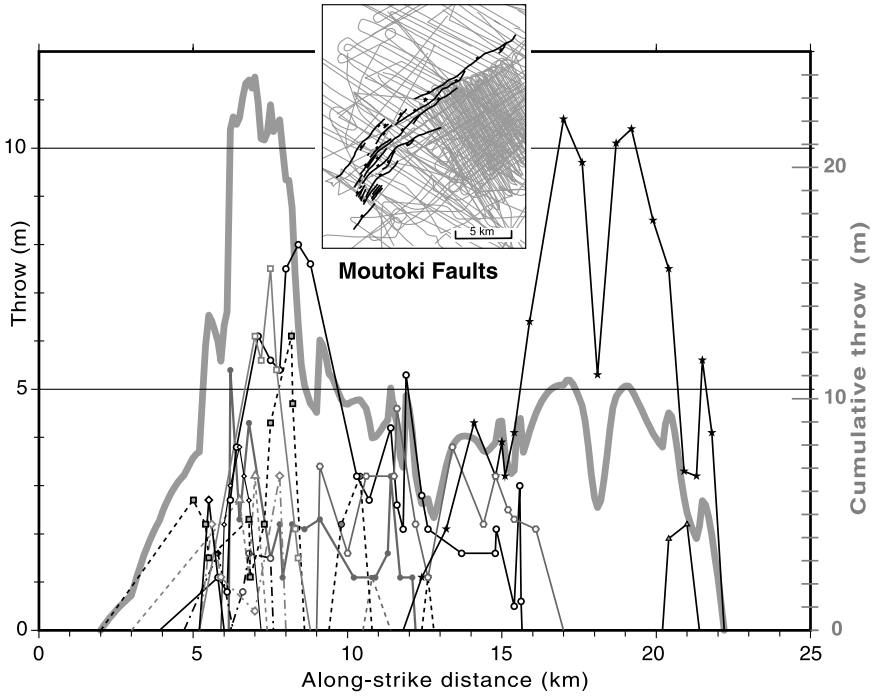

Figure 6. Vertical separation (throw) profiles along the strike of the Moutoki Faults (see Figure 4) for horizon HRS4. Throw values are plotted for individual faults at their crossing point with high-resolution seismic profiles, projected on a strike-parallel axis (see insert). The cumulative throw profile (thick gray line; right-hand-scale) is calculated after decimation of all individual throw profiles in 100 m segments. Insert shows seismic coverage (light gray) of the Moutoki Faults.

VR ± 0.5 mm yr^{-1} on the subsidence or uplift rate. The resulting uncertainty on t_0 is 20%. The error on fault slip rates is taken as the maximum of the error on horizon ages and throws, and can be as high as 35%.

6. Post-20 ka Structure of the Whakatane Graben

[29] The offshore structure is best described as a series of half grabens, characterized by a series of major NW dipping faults, associated with numerous, usually short (<5 km), antithetic SE dipping faults, distributed between the White Island Fault and Tarawera Fault (new name), to the east and west, respectively (Figure 4). The isopach map of sediment above HRS4 (Figure 7) demonstrates that the Rangitaiki and White Island faults are the major structural elements controlling the locus of subsidence, and sedimentation over the last 20 kyr. *Taylor et al.* [2004] demonstrated that these two faults are also the dominant structural elements over more than 1 Myr. In the following, we provide an overview of the faults in the Whakatane Graben. Detailed descriptions of individual fault zones will be published elsewhere, and their relative importance in accommodating strain is addressed in section 8.

6.1. White Island Fault

[30] The White Island Fault projects on land approximately along strike of the Edgecumbe and Te Teko faults (Figure 4), and extends more than 50 km beneath the continental shelf. The surface trace consists of linear segments with an average N40°–45°E trend and two conspicuous corners in the center (C1 and C2 on Figure 4). The bathymetric expression of the fault varies considerably, from no scarp in the south (Figure 8c), to a ~25-m-high scarp in the center (Figure 9b), and a prominent 80-m-high scarp north of C2 (Figures 10a and 11a). In its center, where the White Island Fault interacts with adjacent structures in the graben, the surface displacement becomes highly distributed (Figures 10b, 11b, and 12). At depth, the White Island Fault evolves northward from a single fault in the coastal zone (Figure 8a) to several upward branching splays with antithetic faulting occurring in the hanging wall north of Motuhora Island (Figures 9a and 10a). The vertical separation of the basement surface varies significantly along the fault strike from 0.5 s (~500 m) in the coastal zone (Figure 8a) to about 2 s (~2000 m) near White Island Canyon.

[31] The displacement of the HRS4 horizon across the White Island Fault also varies significantly (Figures 8c, 9b, 10c, and 11a). North of Motuhora Island, the fault displaces postglacial sediments (<17 ka in this area) up to about 40 m in thickness, where the seafloor scarp is about 20 m high (Figures 7 and 9b). Considering the possibilities that all, or none, of the present surface scarp existed at the time of formation of HRS4, and assuming that the postglacial hanging wall sediment thickness represents the minimum accommodation space created by throw on the fault since

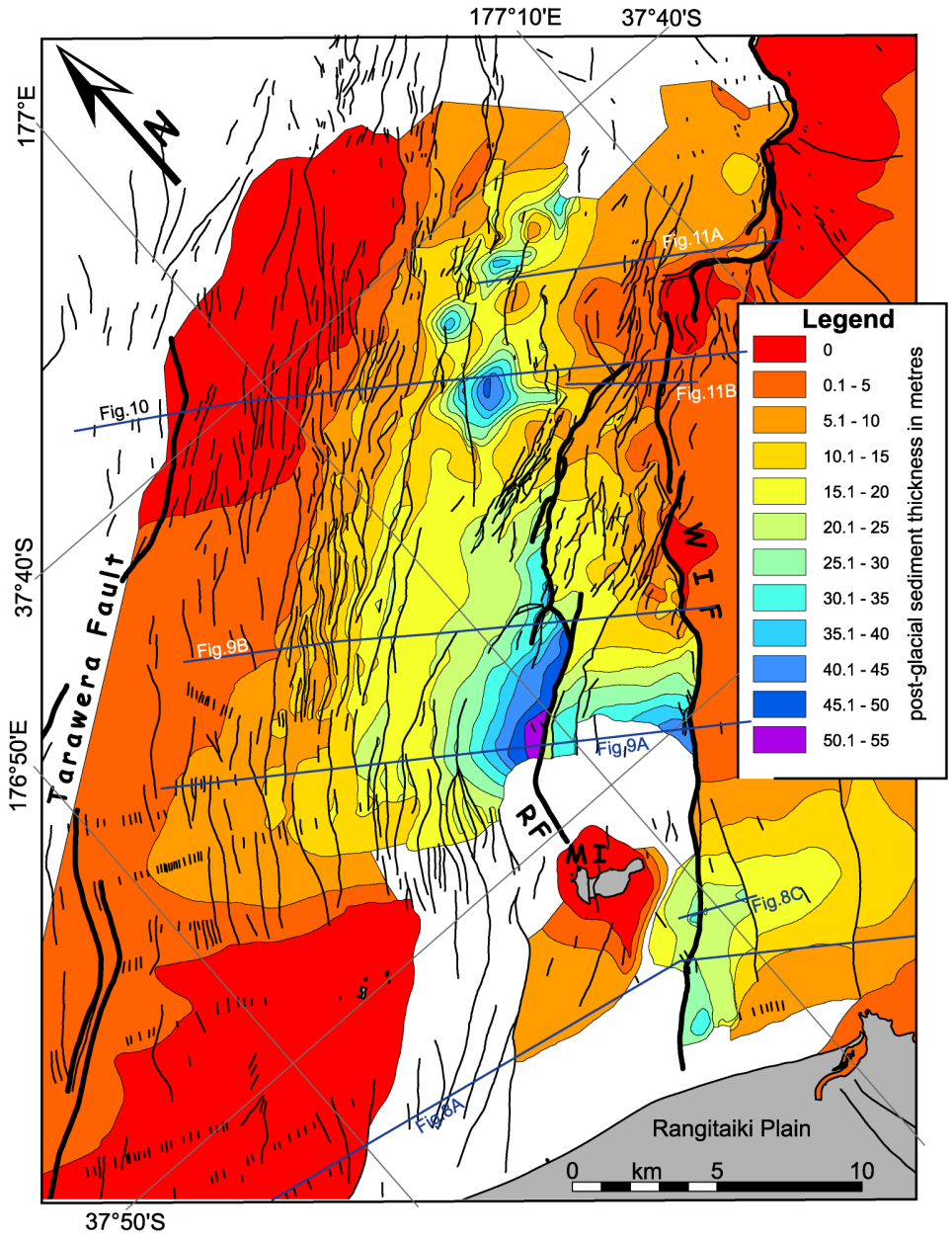

Figure 7. Isopach of the postglacial (<20.5 ka) sediments (above HRS4). Note the figure is rotated so that the axis of the graben runs along the length of the page, and north is oblique. The maximum sedimentation is concentrated in the hanging wall of the Rangitaiki (RF) and White Island (WIF) faults. The maximum thickness of 54 m is seen in the hanging wall of the Rangitaiki Fault, and greater thicknesses may occur farther south closer to Motuhora Island but are not imaged due to the presence of shallow gas. The structural boundaries of the Whakatane Graben to the east and west are highlighted in thick bold lines. MI, Motuhora Island.

HRS4 developed, we estimate a maximum vertical separation rate of up to 2.3–3.5 mm yr^{-1} (Table 1). This upper limit in the displacement rate on this section of the fault compares with a rate of 1 mm yr^{-1} estimated by *Wright* [1990] and *Taylor* [2003]. The increased scarp height near the head of White Island Canyon suggests that vertical displacement rates may increase northeastward.

6.2. Central Graben Faults

[32] The average trend of the central (axial) faults is N56°E (Table 1 and rose diagrams in Figure 4), which is oblique to the White Island Fault (Table 1). In the coastal zone, the South Motuhora and Thornton faults consist of seven large NW dipping structures (Figure 8a), across which the basement drops westward from 0.6 to ~1.8 s

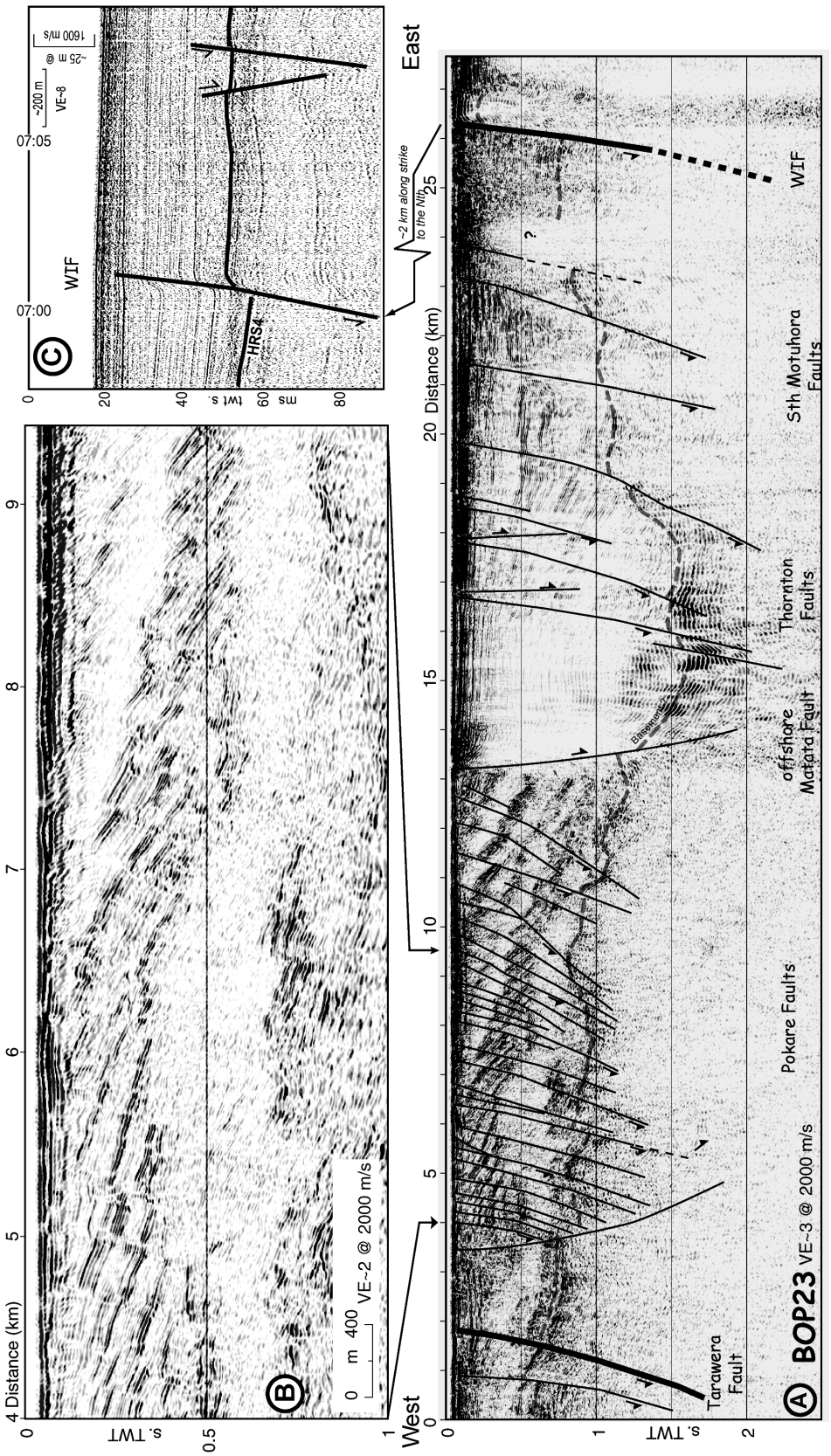

Figure 8. Seismic reflection profiles across the Whakatane Graben within 5 km of the coast. (a) Interpreted migrated MCS section BOP23. There is no reliable correlation with the stratigraphic markers identified in the center of the graben north of Motuhora Island. The eastern and western structural boundaries of the Whakatane Graben are highlighted in bold (Tarawera and White Island faults, Figure 4). The patch of high-amplitude, ringy reflectors at 1.8 s in the middle of the section may represent the graywacke basement but cannot be confidently interpreted eastward across the White Island Fault on this section. Geological outcrops from the margins of the graben on land, together with borehole data from 3.5 to 8 km inland, indicate that approximately the upper half of the sequence consists of pumiceous alluvium, gravels, and ignimbrites, overlying marine sediments of Pleistocene (Castlecliffian) age. This section includes the 0.34 Ma Matahina Ignimbrites overlying Pleistocene strata, but horizon picks are uncertain. (b) Enlargement of reduced vertical exaggeration of the multichannel profile. (c) High-resolution seismic reflection profile (Uniboom source) across the White Island Fault (Line KAH16). The age of HRS4 at that location is 10.6 ± 1.0 ka (see text for method of estimating age of HRS4).

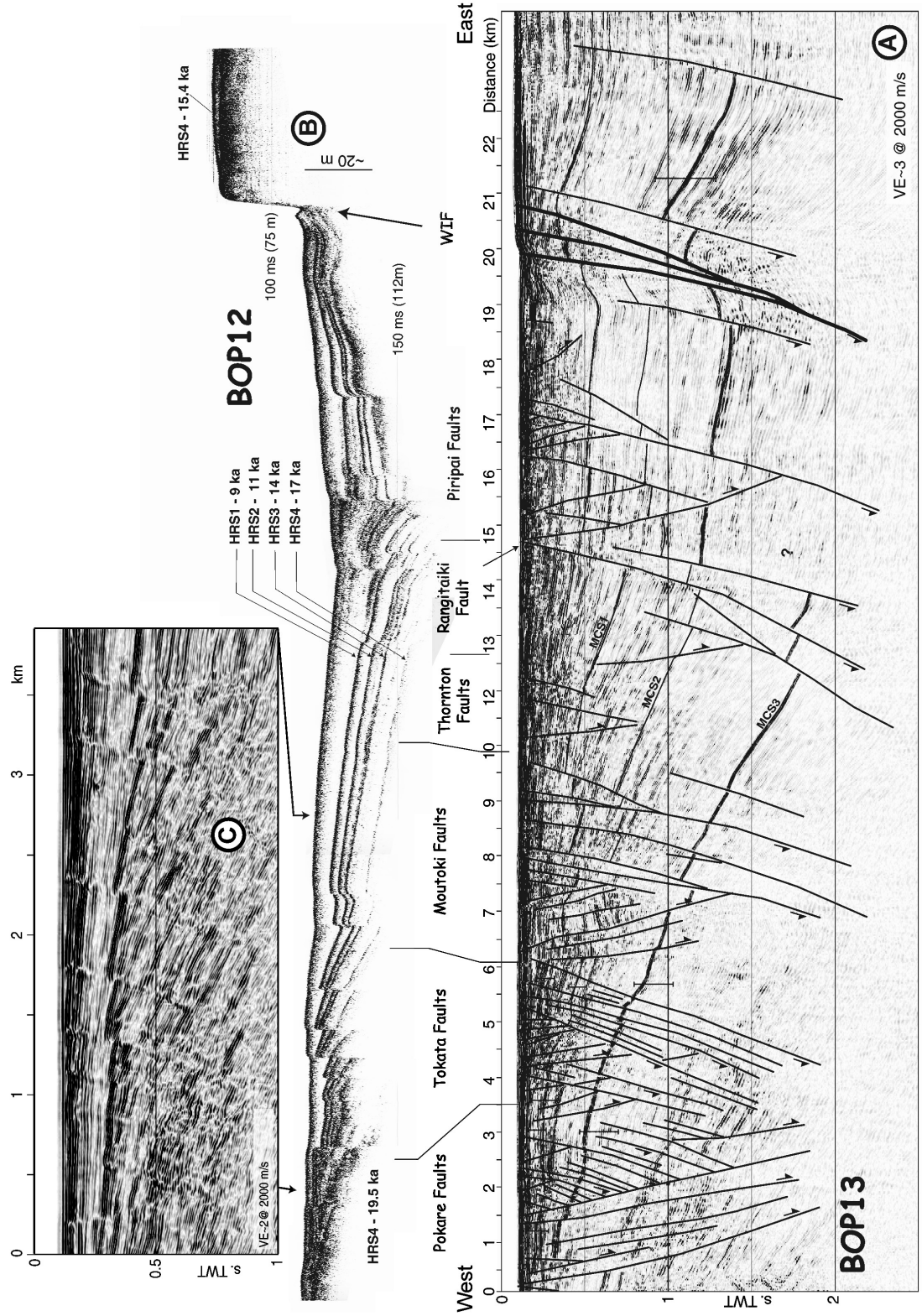

Figure 9. Seismic reflection profiles across the central part of the Whakatane Graben. Location is shown on Figures 3 and 4. (a) Interpreted migrated MCS section BOP13, with MCS1 (300 ± 100 ka), MCS2 (770 ± 290 ka), and MCS3 (1340 ± 510 ka) stratigraphic markers recognized in the center of the graben [*Taylor et al.*, 2004]. The White Island Fault representing the eastern boundary of the graben is highlighted in bold. (b) High-resolution seismic reflection (3.5 kHz) profile of line BOP12. Note the variation of HRS4 age across the graben. (c) Enlargement of migrated MCS profile BOP12 with reduced vertical exaggeration.

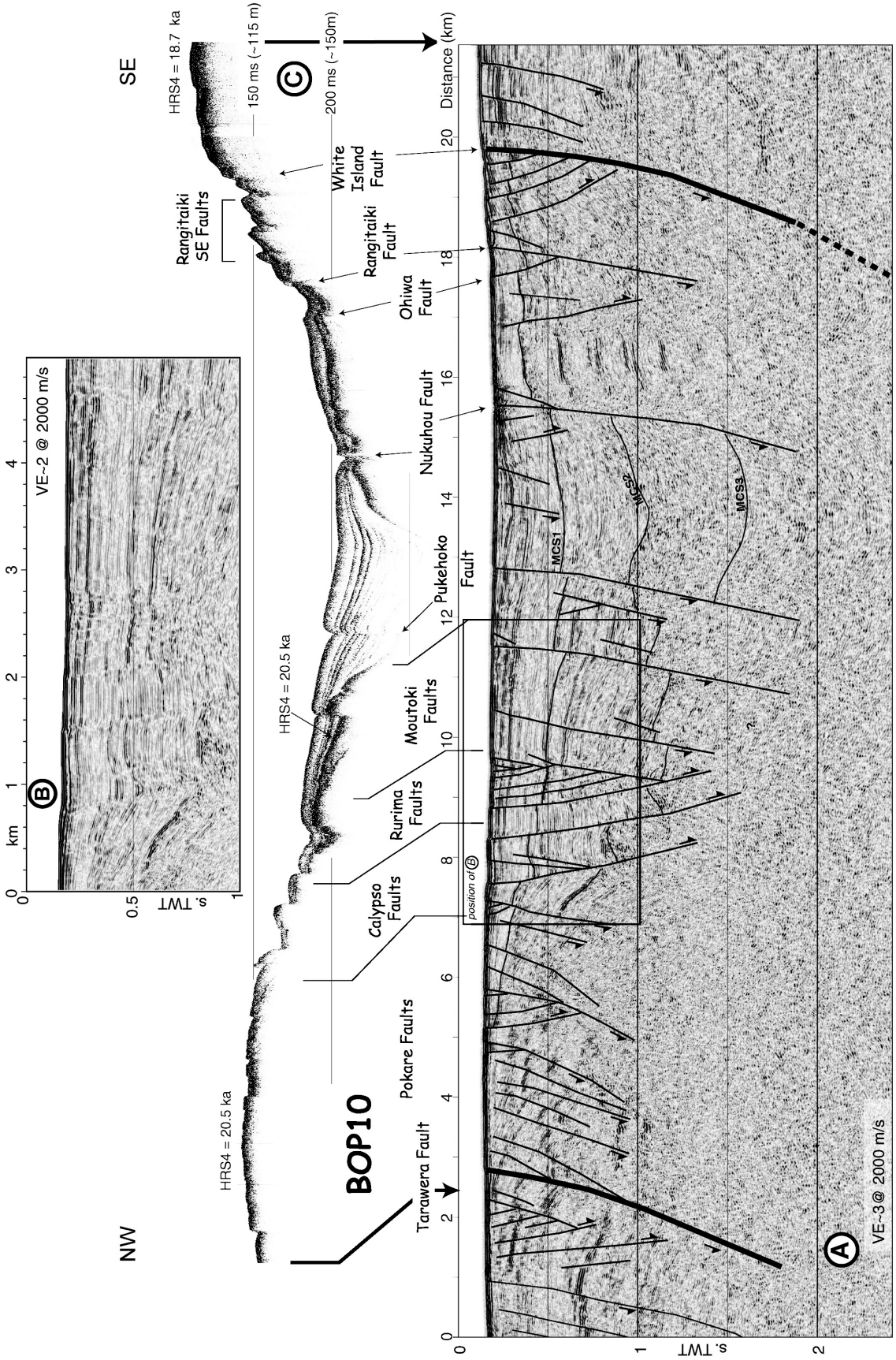

Figure 10. Seismic reflection profiles across the central part of the Whakatane Graben. (a) Interpreted migrated MCS section BOP10. (b) Enlargement of reduced vertical exaggeration over the Rurima and Calypso Faults. (c) High-resolution seismic reflection (3.5 kHz) BOP10.

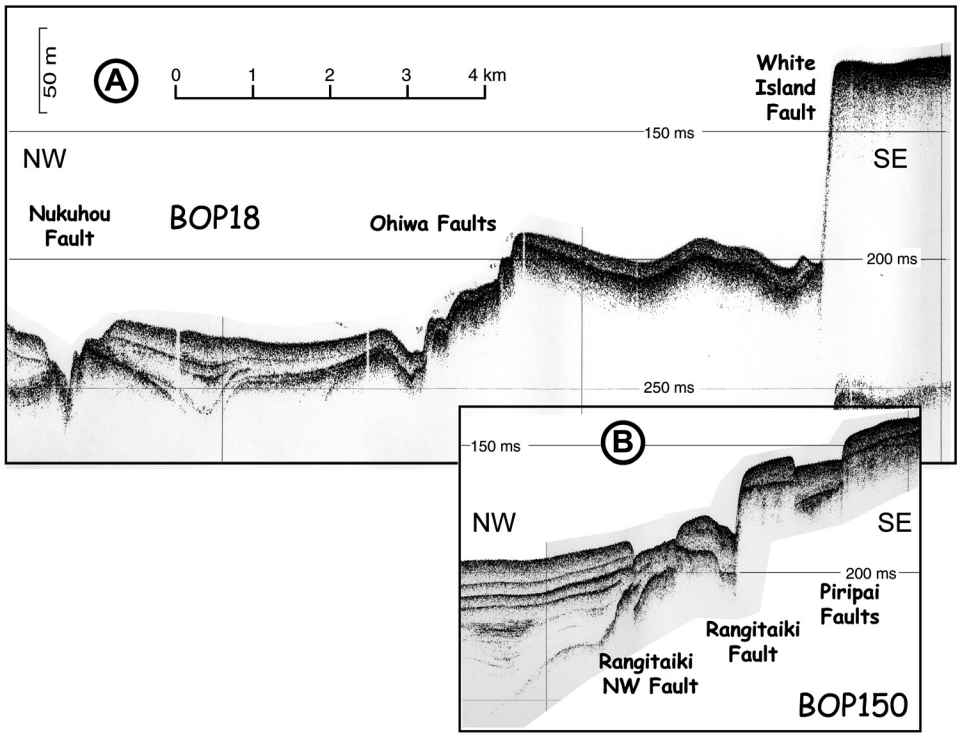

Figure 11. High-resolution seismic (3.5 kHz) reflection profiles (a) BOP18 and (b) BOP150 across the White Island Fault scarp and Rangitaiki Faults, respectively. Location is shown on Figure 4.

(1800 m), in agreement with a cross section on land constructed by *Nairn and Beanland* [1989]. The Thornton Faults project on land approximately along strike of the Awaiti Fault. Northward the fault extends across the shallow platform between Motuhora and Rurima islands, with a noticeable en echelon pattern overlapping the Moutoki Faults to the west. Displacements of up to 10 m of the HRS4 horizon (12–7.5 ka in this sector) yield vertical separation rates of 0.4 and 1.9 mm yr^{-1}, for the South Motuhora and Thornton faults, respectively (Table 1).

[33] North of Motuhora Island, the deformation concentrates along the major 20-km-long Rangitaiki Fault. *Taylor et al.* [2004] showed that the fault has been actively growing for the last 1300 kyr (MCS3), and developed from five segments that linked together between about 300 and 18 ka. *Bull et al.* [2006] have demonstrated temporal and spatial variability in displacement accumulation on the fault since 18 ka and interpreted the data to indicate variable earthquake behavior. The Rangitaiki Fault is associated with the Piripai and Rangitaiki NW fault arrays, to the east (footwall) and NW (hanging wall), respectively (Figures 4, 10, and 11b). The Rangitaiki NW and Piripai fault systems consist of clusters of short (<5 km) antithetic and synthetic faults, except to the SE where one strand of the Piripai Fault extends in isolation for 7 km, but lacks a significant growth sequence in the upper 1.5 s (Figure 9a). Vertical displacement of MCS3 (1340 ± 510 ka) varies considerably along and across strike, with a maximum of 800 m in the center of the Rangitaiki Fault, 400 m across the Piripai Faults and 600 m across the Rangitaiki NW Faults. The Piripai and White Island faults intersect in several places (Figures 4 and 12a), and *Taylor* [2003] suggested that they formed a unique fault zone, prior to hard linkage of isolated segments of the White Island Fault. To the northeast, toward the Ohiwa Fault zone, the Rangitaiki, Piripai and White Island faults converge in a complex zone of distributed deformation and reduced sedimentation (Figures 11 and 12).

[34] The high rate of postglacial vertical displacement on the Rangitaiki Fault is reflected by the main postglacial depocenter being located along its hanging wall (Figure 7), and a vertical separation of HRS4 of >60 m (Figure 9b). Considering the age of HRS4 increases from 15.8 to 18.9 ka along the strike the Rangitaiki Fault, the maximum postglacial vertical separation rate is 3.4 mm yr^{-1} (Table 1). This is about three times the rate prior to development of the fully linked (five segments) fault network [*Taylor et al.*, 2004]. Cumulative vertical displacements of HRS4 of 20 m and 40 m across the Piripai and Rangitaiki NW fault arrays (Table 1), yield vertical slip rates of 1.1 and 2.2 mm yr^{-1}, respectively.

[35] The steep walls of the White Island Canyon make correlation of seafloor scarps with active faults difficult in places, beneath the outer continental shelf. The Ohiwa Faults consist of several antithetic faults in the southwest, which connect with the northern end of the Rangitaiki Fault (e.g., Figure 12a). In contrast, the Nukuhou Faults consists of the 10 discrete isolated faults displacing a sequence of postglacial sediments about 10 to 30 m thick (Figure 7). The cumulative displacements of HRS4 (20.5 ka in the area) across the Ohiwa (57 m) and Nukuhou faults (27 m) result

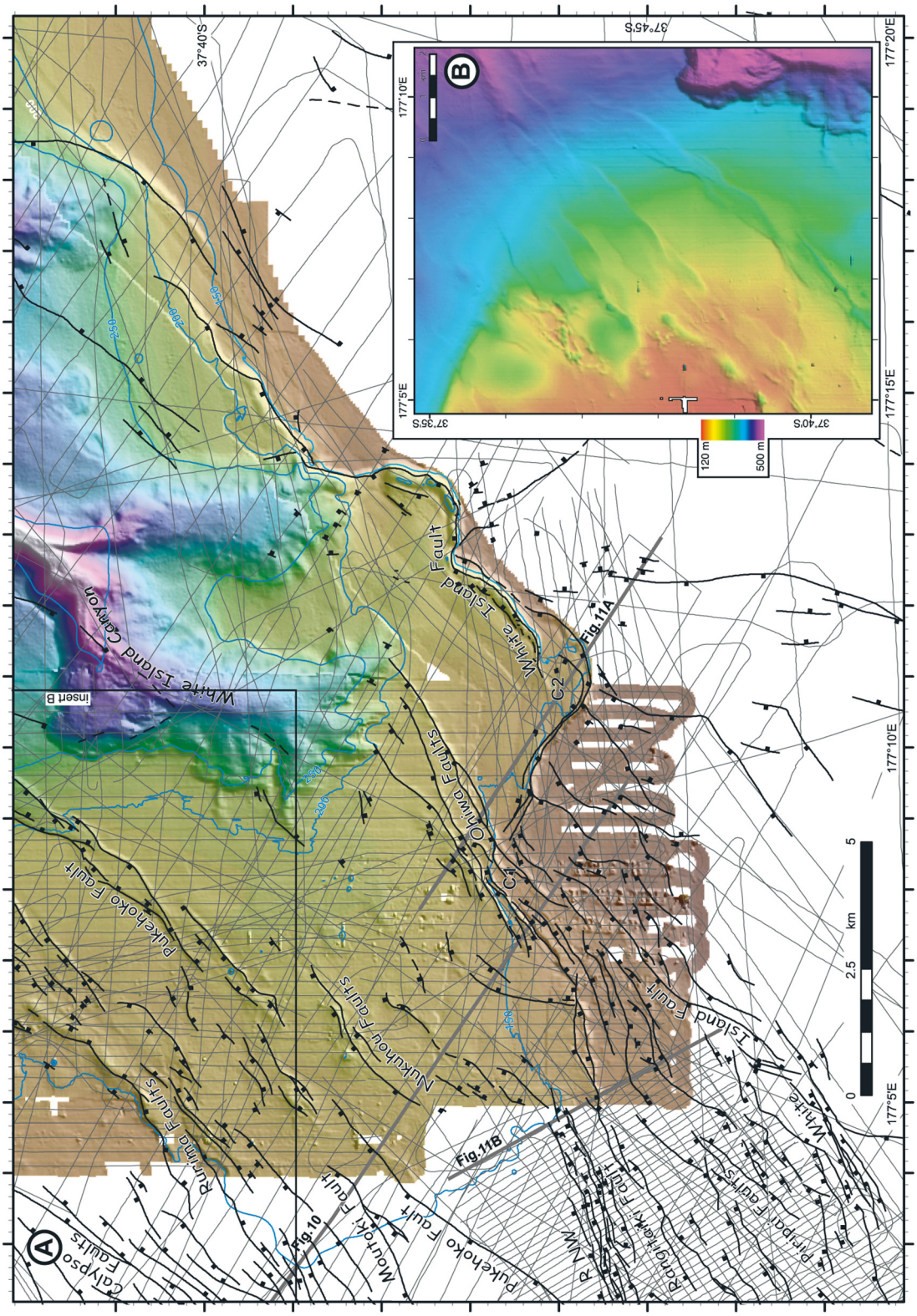

Figure 12. (a) Swath bathymetry and active faults over the eastern boundary of the Whakatane Graben and along the northern part of the White Island Fault. Ticks along faults indicate displacement sense. Light gray lines indicate high-resolution seismic (3.5 kHz) data utilized for interpretation of fault dip (some editing was undertaken for clarity). Illumination is from N315°E. C1, C2 are White Island Fault trace corners (see text). (b) Uninterpreted region of multibeam data, over the north part of the graben (see location on Figure 4).

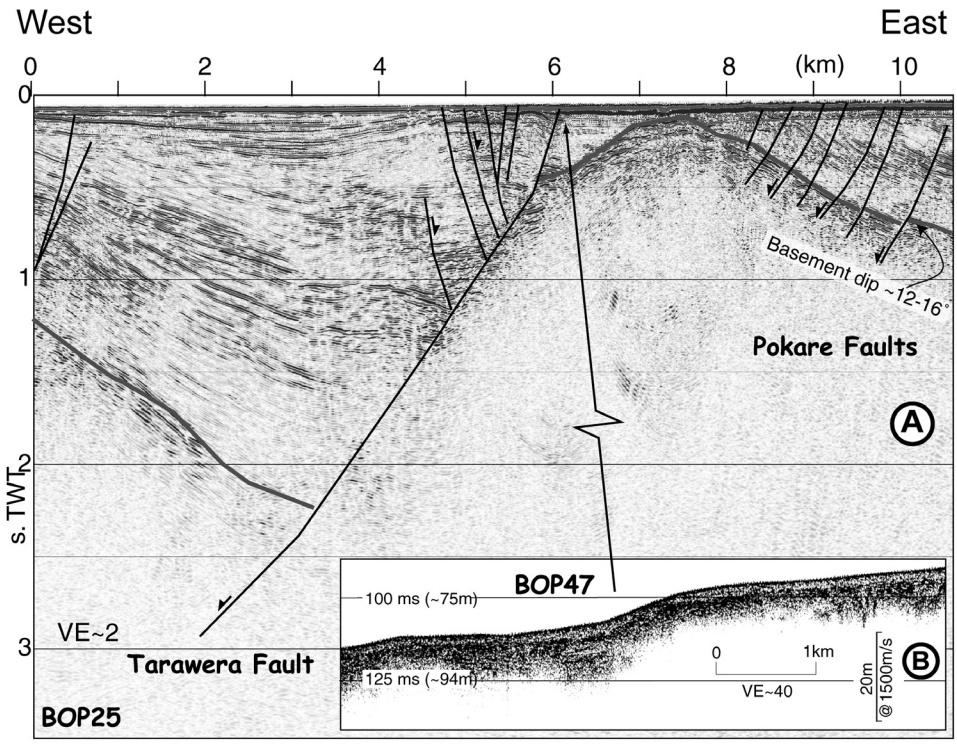

Figure 13. (a) Interpreted MCS reflection profile BOP25 across the Tarawera Fault. The Tarawera Fault represents the western boundary of the Whakatane Graben (locations on Figures 3 and 4). (b) The 3.5 kHz profile BOP47, across the Tarawera Fault, ~8 km northeast of line BOP25.

in maximum vertical separation rates of 2.8 and 1.3 mm yr^{-1}, respectively (Table 1). This compares with a rate of 0.7 ± 0.3 mm yr^{-1} determined by *Wright* [1990] on selected components of the Ohiwa Fault zone.

6.3. Rurima Ridge

[36] The six fault zones identified beneath the Rurima Ridge (Moutoki, Tokata, Pukehoko, Rurima, Calipso, and Pokare faults), developed in the back limb of large basement blocks (Figure 13). The true dip of the basement surface is estimated between 12° and 16°. The average fault strike is N46°E (Figure 4), which is oblique to the average fault orientation in the center of the graben, but is subparallel to the White Island Fault. In contrast with the center of the graben, SE dipping (antithetic) faults often display the longest surface scarps (e.g., the Tokata and Calypso faults; Figure 4), and merge at depth with larger NW dipping faults typically within the 1.5 km (1.5 s) (Figure 9a), but possibly up to 2–4 km (>2.5 s) in places (Figure 10a). Domino fault arrays (Figures 8a and 8c) are observed in the south (Figures 8a, 8c, and 10a).

[37] Shallow water depths (<50 m) in the coastal zone, combined with the presence of unconsolidated gas-rich mud in the upper surface resulted in reduced resolution and penetration, and poor correlation across the seismic network of small-offset faults observed on the shallow platform south and west of the Rurima Islands (Figures 4, 8a, and 8c). Two large east dipping faults, west of the graben center (Figure 8), project into the Matata Faults to the south, and the Moutoki and Tokata faults to the north. The Moutoki and Tokata faults form a dense and complex deformation zone with faults dipping both to the SE and to the NW (Figure 9a). Some of the antithetic faults have surface traces extending up to 13 km. Both fault zones extend approximately 20 km to the NE and have similar maximum vertical displacements of the HRS4 surface in the order of 7 to 10 m (Table 1). The cumulative displacements of HRS4 across the Moutoki and Tokata fault zones yield vertical slip rates of 1.5 and 1.9 mm yr^{-1}, respectively.

[38] In map view, the Moutoki Fault Zone is characterized by left stepping, en echelon fault traces, that overlap the Pukehoko and Rurima faults zones. The Pukehoko Faults extend for more than 22 km beneath the eastern flank of the Rurima Ridge, and consists of five major segments up to 8 km in length (Figure 4). The fault displaces postglacial (<20.5 ka) sediments, up to 45 m thick (Figure 7), and is associated with surface bathymetric scarps up to 14 m high (Figure 10c). The cumulative vertical displacement of HRS4 across the Pukehoko Faults indicates a maximum vertical separation rate of 1.7 mm yr^{-1} (Table 1).

[39] The Rurima (including the Rurima Fault in the sense of *Wright* [1990]) and Calypso faults, extend for more than 20 km beneath the axis of the northern part of Rurima Ridge, and consist of more than 40 fault traces mainly dipping east. At depth, the faults likely intersect with the Moutoki Faults to the south, and the Pukehoko Faults to the

northeast (Figure 10a). In the northeast, the fault zones narrow and become part of an array of principally northwest dipping structures, which include the Pukehoko and Pokare faults. The faults displace a condensed postglacial sedimentary sequence (Figures 7 and 10c). The HRS4 (circa 20.5 ka) cumulative vertical displacement of 50 and 27 m, yield maximum vertical separation rates of 2.6 and 1.4 mm yr^{-1}, for the Rurima and Calypso faults, respectively (Table 1).

6.4. Tarawera Fault

[40] The Tarawera Fault zone represents the western margin of the Whakatane Graben. It is defined by a series of major faults dipping to the northwest, which extend from near the coast 10 km west of Matata, toward White Island (Figure 4). It is separated from the Moutoki and Tokata faults by the Pokare Faults, a corridor of poorly correlated structures (Figures 9a and 10a). Estimate of cumulative displacements of HRS4 across the Pokare Faults yield a maximum cumulative vertical separation rate of 1.6 mm yr^{-1} (Table 1). The Tarawera Fault separates the shallow basement surface beneath Rurima Ridge from a significant growth sequence up to 2.5 s in thickness ($\sim$2.5 km) in the hanging wall (Figures 9 and 13). The fault is associated with seabed traces up to 15 km in length, and surface scarps of 4 m in height (Figures 9c and 13b). A maximum throw of the HRS4 surface of 11 m yields a current vertical slip rate of 0.55 mm yr^{-1} which is not more than half of the average long-term rate assuming the fault is less than 1.6 Myr old. Northward, the Tarawera Fault divides in multiple strands converging toward the Rurima and Calypso faults when approaching White Island (Figure 4).

7. Cumulative Throw and Vertical Separation Rates

[41] We determine the incremental cumulative throw of HRS4 along four parallel 30-km-long transects running northwest to southeast, perpendicular to the graben axis, from the Tarawera Fault to the White Island Fault (Figure 14a). The maximum cumulative vertical displacement exceeds 160 ± 30 m. The southern transect (T1) systematically shows lower throws than the other transects. The total cumulative displacement on T1 is 61 ± 12 m, which is less than half of the average value of 150 ± 30 m measured on profiles T2 to T4 (Table 2). The low displacements along T1 are partly explained by the poor resolution and low penetration on high-resolution seismic profiles, resulting from gas masking of HRS4. Hence the displacements on T1 are considered minimum values, and we use the median value of 143 ± 29 m as representative of the total cumulative vertical displacement across the graben.

[42] The cumulative vertical displacement across Rurima Ridge is 37 m on T1 and 50 m on average on T2, T3 and T4, with a maximum throw of 7 m across any individual faults (Figure 14a). Across the center of the graben the displacements cumulate to 22 m on T1 and 84 m on T3. The maximum throw on any individual structure is 32 m across the Rangitaiki Fault on T2, south of the maximum displacement of $\sim$60 m, which represents 25% of the total cumulative displacement along the transect. The maximum displacement observed across the White Island Fault is 2.3 m on T1, and up to 40 m on T4.

[43] Because HRS4 is diachronous, it is essential to normalize the displacements along the transects by the age of HRS4 (t_0) at the location of each measurement. The resulting vertical separation rates are nearly coincident for the four profiles (Figure 14b and Table 2). The total cumulative vertical separation rates at the surface on transects T1 to T4 range from 5.0 ± 1.3 to 8.1 ± 2.0 mm yr^{-1}, respectively. We believe the median value of 8.0 ± 2.0 mm yr^{-1} is representative of the surface throw rate across the graben. Although displacements across the Rangitaiki and White Island faults on transect T2 represents 50% of the total displacement across the graben, the cumulative rates on T2, T3 and T4 are almost identical. This suggests that extensional strain is accommodated consistently across the graben. The median cumulative surface dip-slip rate across the graben, calculated using an average fault dip of 70°, is 8.5 ± 1.9 mm yr^{-1}.

8. Discussion

8.1. Rifting Obliquity and Structural Style

[44] The new fault map, combined with the dense grid of variable resolution seismic reflection profiles in the offshore Whakatane Graben, provides a three-dimensional structural resolution not previously available in the Taupo Volcanic Zone, and rarely available in other active continental rifts. Overall our interpretation, together with the seismic profile documented by *Davey et al.* [1995], show that the offshore structure of the rift is more appropriately described as a series of half grabens. This asymmetry differs not only from the onshore and coastal (Figure 8a) Whakatane Graben, but from active rifting along the greater Taupo Volcanic Zone on land, which have been described as symmetrical grabens [*Rowland and Sibson*, 2001; *Villamor and Berryman*, 2001].

[45] The major faults in the Whakatane Graben illustrate variations in the degree of segmentation and linkage. There is a noticeable northward, left-lateral en echelon pattern across the Thornton and Moutoki fault groups, where faults largely overlap, but are not linked at the surface. We infer that the displacement is transferred between fault segments across gently dipping relay ramps. Only one such ramp on the northern part of the Moutoki Faults appears to have been breached by a transfer fault that has propagated from the tip of the rear trace, linking two segments (location R1 in Figure 5). In comparison, all of the major left-stepping segments of the more active Rangitaiki Fault became fully linked between 300 and 18 ka, in association with an increase in the fault's displacement rate [*Taylor et al.*, 2004]. This linkage occurred by breaching of initial relay ramps up to 2 km wide (e.g., R2, Figure 5).

[46] There is no evidence for cross faults striking at a high angle to the axis of the rift. In some other rift systems, such faults include strike-slip or oblique-slip structures that link offset compartments of the rift [e.g., *Gibbs*, 1990; *Scott et al.*, 1992; *McClay and Khalil*, 1998]. Several of the

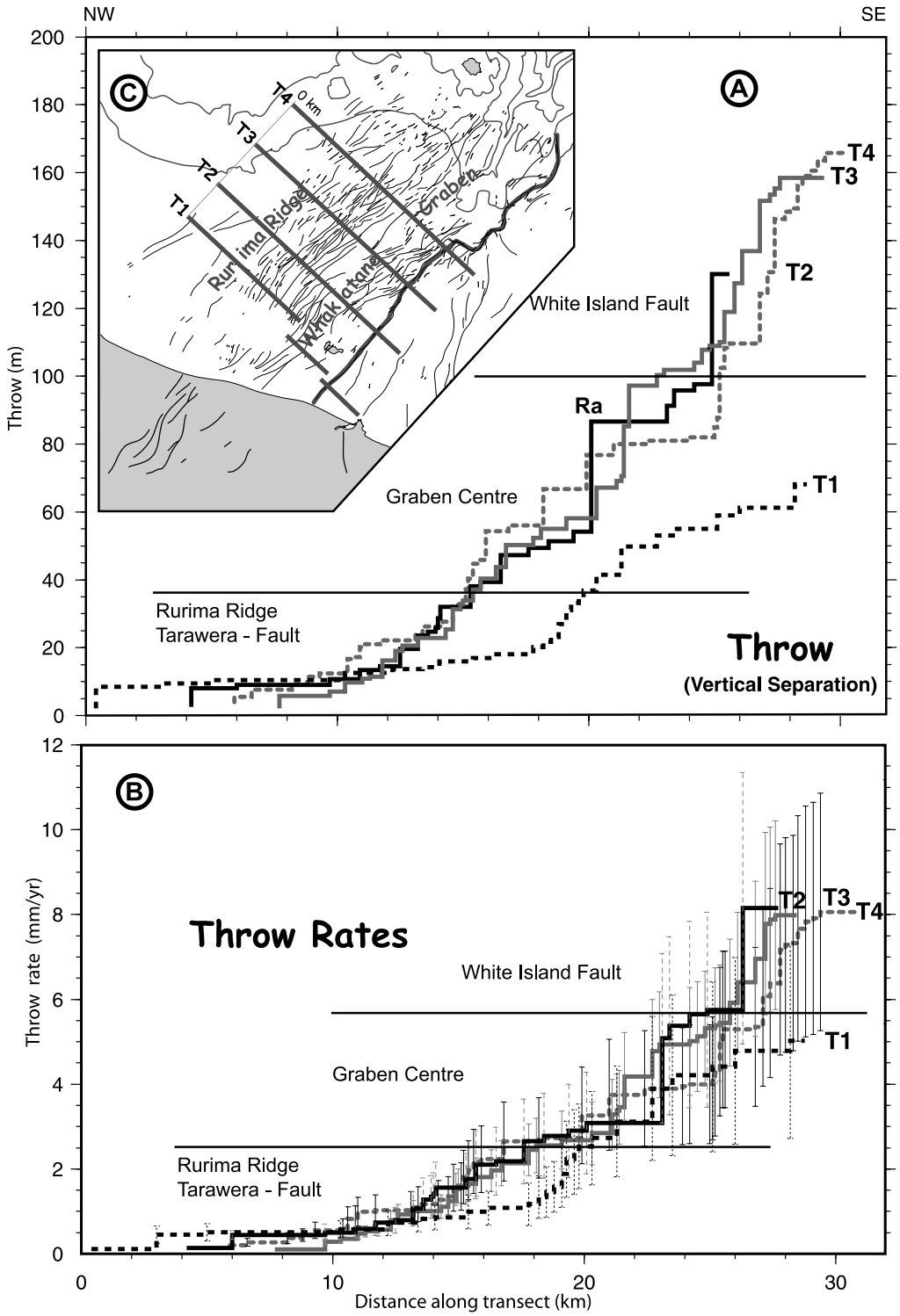

Figure 14. Post-20 ka accumulation of (a) vertical displacements and (b) rates along NW-SE graben-normal transects. Vertical separations (throw) are projected from the nearest measurement on a seismic profile. The measurements are typically <500 m, and always <1500 m from the transects. Measurements from multiple equidistant profiles are averaged. On Rurima Ridge and east of the White Island Fault where seafloor and HRS4 are coincident, i.e., post last glacial sediment is absent (Figure 7), seafloor displacements are assumed to be post-HRS4 in age. Transect origins are aligned parallel with the axis of the graben, with T1 origin immediately west of the Tarawera Fault. The Rangitaiki Fault (RF) is indicated on the vertical displacement profiles. (c) Locations of transects. The White Island Fault is highlighted in bold.

Table 2. Post-20 ka Displacement and Extension Rates Across the Whakatane Graben[a]

		Surface Rates, mm yr^{-1}			Rates at Seismogenic Depth, mm yr^{-1}			
	Throw, m	Throw (TR)	Dip Slip (SDS)	Extension (SER)	Dip slip (1.6 Factor) (DSR)	Extension (ESR)	Extension With Small EQ Correction (1.3) (CER)	Dextral Component (Dext)
T1	61 ± 12	5.0 ± 1.3	5.3 ± 1.3	1.8 ± 0.5	8.5 ± 2.1	6.0 ± 2.5	7.9 ± 3.5	2.9 ± 1.3
T2	130 ± 26	8.2 ± 2.0	8.7 ± 2.2	3.0 ± 0.7	13.9 ± 3.5	9.8 ± 2.5	12.8 ± 5.7	4.6 ± 2.1
T3	155 ± 31	8.0 ± 2.0	8.5 ± 2.1	2.9 ± 0.7	13.6 ± 3.4	9.6 ± 2.4	12.5 ± 5.6	4.5 ± 2.0
T4	164 ± 33	8.1 ± 2.0	8.6 ± 2.1	2.9 ± 0.7	13.7 ± 3.4	9.7 ± 2.4	12.6 ± 5.7	4.6 ± 2.1
Med	**143 ± 29**	**8.0 ± 1.8**	**8.5 ± 1.9**	**2.9 ± 0.7**	**13.7 ± 3.1**	**9.7 ± 2.5**	**12.6 ± 5.7**	**4.6 ± 2.1**
TFB-60°		**7.2 ± 0.4**	7.5 ± 1.9	1.9 ± 0.5	12.0 ± 4.4	6.0 ± 3.1	7.8 ± 3.5	
TFB-45°		**7.2 ± 0.4**	7.7 ± 1.9	2.6 ± 0.7	12.3 ± 4.5	8.7 ± 3.2	11.3 ± 5.1	

[a]Rates are calculated along the four transects (T1 to T4) generated perpendicular to the graben axis (Figure 14). Throw rates (TR) are calculated using our new estimate of the age of HRS4 (t_0) with TR = Th/t_0, with Th being throw. Surface dip-slip (SDS) and extension rates SER calculated using an average fault dip of 70° (SDS = Th/sin(70°) and SER = Th/tan(70°)). We estimate a 25% uncertainty associated with measurement errors (see section 5.1) and fault dips ranging 65–75°. Dip-slip rates (DSR) at seismogenic depth (6–10 km) are calculated by applying a correction of 1.6 to surface measurements so as to compensate for the discrepancy between surface and crustal displacements for large earthquakes [*Villamor and Berryman*, 2001], and see text for explanation. Note that these dip-slip measurements are independent of crustal fault dip. Extension rates at seismogenic depth (ERS) calculated using a fault dip of 45° at crustal depth (ERS = DSR cos(45°) = 1.6 SER cos(45°)), with quoted errors including an error of 15% on the fault dip and errors carried from surface estimates. An additional correction of 1.3 applied to crustal extension rates to compensate for the contribution of small earthquakes [*Villamor and Berryman*, 2001], providing the corrected extension rate at seismogenic depth (CER = 1.3 SER). Displacements from both synthetic and antithetic faults are taken into account. Dextral component (Dext) calculated using a ~20° rift obliquity to the direction of extension (Dext = CER tan(20°)). Errors on rates at seismogenic depth are calculated with minimum and maximum values from surface rates. Values in bold are median values, thus not biased toward transect T1, in which low values are associated with poor data. We recalculate the dip-slip and extension rates in the Taupo Fault Belt from published throw rates [*Villamor and Berryman*, 2001], using all faults (i.e., including antithetic), and the 75° and 60° published fault dips at the surface and at depth, respectively (TFB-60°), as we believe Villamor and Berryman's calculations (their Table 5) contained some errors. We also calculate the rate in the TFB using surface and crustal fault dip estimates of 70° and 45° (TFB-45°).

obliquely striking axial faults in the Whakatane Graben, however, interact with the eastern margin of the rift, resulting in local perturbations in the strike of the White Island Fault. This is notable in the region where the Piripai, Rangitaiki and Ohiwa faults intersect the White Island Fault (Figures 4 and 12).

[47] The question of extension obliquity in the TVZ has significance to kinematic models of North Island tectonics and back-arc or rifted-arc deformation resulting from oblique convergence. While there has recently been debate about the extension direction across four major segments of the active rift south of the Whakatane Graben [*Rowland and Sibson*, 2001; *Acocella et al.*, 2003; *Wallace et al.*, 2004], there is evidence that a degree of oblique extension is occurring in the Whakatane Graben. We estimate the overall trend of the rift axis to be N43°E ± 3°, by considering the topographic and bathymetric expression of the graben, the strike of major faults near the margins, and the axis of postglacial sediment depocenters (Figure 7). The White Island Fault, and faults beneath the axis of Rurima Ridge (Pokare, Tokata, Rurima, and Calypso faults), have mean strikes typically within a few degrees of the overall rift axis (Figure 4 and Table 1). In contrast, the major faults along the axis of the graben have mean strikes typically between N55°E to N60°E, and significant components between N60°E and N70°E. This pattern is mirrored onshore with active faults beneath the Rangitaiki Plain (e.g., Edgecumbe, Awaiti, and Te Teko faults) striking oblique to the Matata faults along the north western margin of the graben (Figure 4).

[48] Two historical earthquakes provide extension directions, expressed as horizontal projections of slip vectors and T axes (Table 3). The extension direction during the M_w 6.5 1987 Edgecumbe earthquake was determined to be N330°E from displaced geomorphology [*Beanland et al.*, 1989, 1995] and N342°E from the main shock focal mechanism [*Anderson and Webb*, 1989]. This direction is approximately perpendicular (i.e., close to dip slip) to the N55°E striking Edgecumbe and Te Teko normal faults (Figure 4), which ruptured during the earthquake to a depth of about 6–8 km [*Anderson et al.*, 1990; *Webb and Anderson*, 1998], causing

Table 3. Earthquake Source Parameters for the Three Large Historical Seismic Events in the Bay of Plenty Region[a]

Name	Date	M_L	Depth	Strike	Dip	Slip	Reference
Bay of Plenty	21 Jun 1992	M_w = 6.3	4 (−1/+2)	32 (−20/+10)	41 ± 5	333 ± 10	*Webb and Anderson* [1998]
Matata	31 May 1977	5.4	10.4	37	80	356	*Richardson* [1989]
Edgecumbe	2 Mar 1987	6.5	6 ± 1	49 ± 10	32 −10/+5	334 ± 6	*Webb and Anderson* [1998]
Edgecumbe	2 Mar 1987	6.5	8 ± 3	45	45 ± 10	342	*Anderson and Webb* [1989]
Edgecumbe	2 Mar 1987	6.5	6.4 ± 1	55	39 ± 3	325	*Darby* [1989]
Edgecumbe	2 Mar 1987	6.5		55	-	330	*Beanland et al.* [1989]

[a]Errors are only indicated where clearly given in the original reference.

subsidence of up to 2 m over some 200 km^2 of the Rangitaiki Plain [*Beanland et al.*, 1989]. The 1977 M_L 5.4 Matata earthquake sequence ruptured an approximately N37°E striking offshore fault with right-lateral and normal slip, to a depth of 10.5 km, and with an extension direction of N356°E [*Richardson*, 1989]. These azimuths compare with extension directions of N340°E [*Rowland and Sibson*, 2001] and N323°E [*Acocella et al.*, 2003], determined from analysis of mesoscopic faults near the northwestern margin of the graben, with various geodetically determined extension azimuths of N300°E ± 16° [*Sissons*, 1979], N323E ± 34 [*Adams*, 1983], N338°E ± 12° [*Walcott*, 1984], and N330°E [*Crook and Hannah*, 1989], and with an extension direction of about N315°E derived from kinematic modeling of GPS and geological data [*Wallace et al.*, 2004]. Assuming equal weight to these data, the average extension direction across the onshore graben is about N330°E, with uncertainty estimated to be about 25°.

[49] The average extension direction from above is about 70° from the overall trend (N43°E ± 3°) of the graben, implying extension obliquity (α) of about 20°. This assessment is in good agreement with the results of *Rowland and Sibson* [2001] and *Acocella et al.* [2003]. The component of right-lateral deformation represents about 36% of the magnitude of orthogonal extension across the graben. Geometric aspects of the rift, both onshore and offshore, reflect the oblique extension. Most notable is the obliquity of the major axial faults relative to the structures on and close to the margins of the graben (Figure 15). This fault pattern, with intrarift structures oriented approximately perpendicular to the extension direction, has striking similarity to rift geometries developed in analogue model experiments with low to moderately oblique extension directions of α = 60–75° [*Tron and Brun*, 1991; *McClay and White*, 1995]. The left-stepping en echelon geometry of the Thornton, Moutoki and Rangitaiki faults is also consistent with experimental results of right-lateral oblique extension [*Richard*, 1991]. Analogous natural rifts considered by *McClay and White* [1995] and *McClay* [1996] to be representative of such extension include the Rukwa Rift of East Africa [*Morley et al.*, 1992] and the Danakil Graben of Afar [*Kronberg*, 1991].

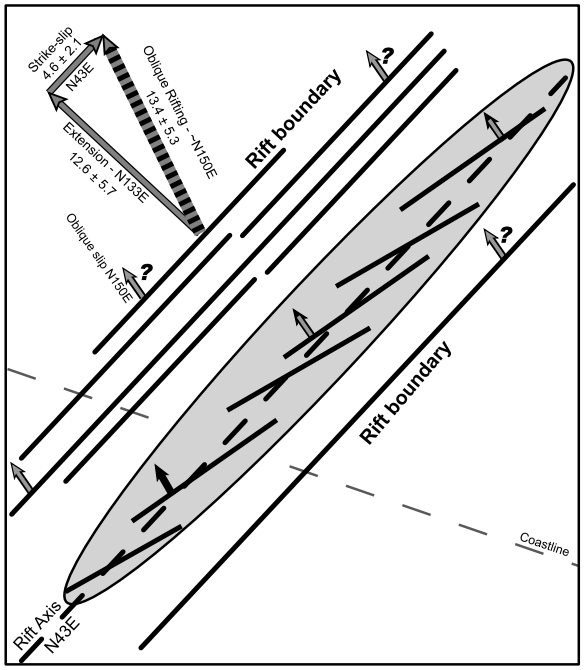

Figure 15. Simple kinematic model of oblique extension in the Whakatane Graben. Faults in the center of the graben are oblique to the rift axis and rupture in pure dip-slip slip displacement events (black arrows [e.g., *Anderson and Webb*, 1989]). Faults near the margins of the rifts are inferred to be oblique slip structures (gray arrows). The coastline is indicated for reference only.

8.2. Extension Rate Across the Whakatane Graben

[50] The offshore seismic profiles reveal that major faults in the basement and lower sedimentary section commonly splay upward into multiple, subparallel surface traces. The steep (~70°) near-surface fault dips, also observed commonly onshore in the TFB [*Villamor and Berryman*, 2001], is attributed to tensional failure of the relatively weak sediments in the upper few tens of meters [e.g., *Jackson and McKenzie*, 1983]. The observed fault geometries are comparable to structures developed in cover sequences during normal fault propagation in experimental clay models [*Withjack et al.*, 1990]. In the case of the Whakatane Graben, seabed traces are associated with both NW and SE dipping faults (i.e., synthetic and antithetic, respectively), which commonly occur in complexly linked conjugate networks within the upper 1.0–2.0 km. While the arrays are dominated by the NW dipping faults, antithetic faults may have comparable or greater post-20 ka displacement rates and trace lengths. A notable example of such behavior is observed along the Tokata Faults. Throws on antithetic faults represent approximately 10–15% of the cumulative vertical displacement along transect T1 to T3, and up to 25% on T4. From the highly distributed and approximately contemporaneous surface deformation, we infer that large earthquakes could be associated with surface ruptures on multiple traces, and unlike *Villamor and Berryman* [2001], we believe that all of the faults displacing horizon HRS4 contribute to the crustal extension accrued since formation of that surface. Consideration of the near-surface dips enable calculation of dip-slip (Dsr) displacement rates (Tables 1 and 2), which are about 10% (i.e., Dsr = throw/cos70°) larger than vertical separation (throw) rates.

[51] The cumulative vertical displacement rates for the post last glacial transgressive surface (HRS4) calculated for the four regional transects (Figure 14) can be used to derive extension rates across the entire width of the Whakatane Graben (Table 2). Because the transects are perpendicular to the mean rift axis, the rates represent the true extension across the rift. We calculate a surface extension rate of 2.9 ± 0.7 mm yr^{-1} (Table 2). In comparison, *Wright* [1990] derived an extension rate of 3.5 ± 1.7 mm yr^{-1} from a sparser set of surface fault throws using an average fault dip of 45°. This value reduces to 1.3 mm yr^{-1}, when using a 70° surface fault dip.

[52] The large earthquakes of Edgecumbe 1987 (M_w6.5) and Bay of Plenty 1992 (M_w6.3) (Figure 4 and Table 3) provide good constraints on the dip of the major faults at seismogenic depths. The preferred centroid moment tensor solution for the offshore 1992 Bay of Plenty earthquake indicates a fault with strike and dip of N32°E (−20/+10) and (41 ± 5)°, respectively [*Webb and Anderson*, 1998]. Estimates of the Edgecumbe Fault dip from the main shock focal mechanism solution range from 45° ± 10° [*Anderson and Webb*, 1989] to 32° +5/−10° [*Webb and Anderson*, 1998], and 39° ± 3° from dislocation modeling [*Darby*, 1989]. These estimates, combined with the observed surface ruptures indicated planar fault geometry, while the earthquake magnitudes and estimates of total basement displacement of 1200 m confirm the fault as representative of the large structures in the graben [*Woodward*, 1989]. Rupture of the entire brittle crust during these earthquakes indicate that if any detachment exists beneath the TVZ, it is in the lower crust and will therefore likely be aseismic. The focal mechanisms, together with the depth-converted estimates of fault dip in the deeper sedimentary cover sequence, are in good agreement with global compilations of large normal fault earthquakes, which are most commonly associated with faults dipping at 30–60° [*Jackson and White*, 1989]. Considering the combined observations from the graben, and global compilations, we estimate that the major, crustal-scale faults in the Whakatane Graben have dips in the range of 45 ± 15°. Such a range is consistent with observed basement blocks now back tilted to dips of up to 12–16° (e.g., Figure 13a), and with geophysical estimates of crustal extension of 1.4–2.0 [*Stern*, 1985; *Harrison and White*, 2004]. The asymmetry of the rift and the planar fault geometry imply a domino style extension in which both the basement blocks and the faults rotate about a horizontal axis with increasing extension and crustal thinning [*Jackson*, 1987]. Our observation of domino faulting in the western part of the Whakatane Graben is further evidence that fault rotation has occurred, which support our interpretation of fault dip less than the theoretical (60°) ''Andersonian'' dip predicted for young faults in a homogeneous medium.

[53] We follow a similar line of reasoning as that of *Villamor and Berryman* [2001] to derive the extension rate at the crustal depth of 6–10 km by applying two correction factors to our surface measurements (Table 2). Empirical relationships between surface and subsurface displacements associated with historical earthquakes [*Wells and Coppersmith*, 1994] suggest that displacement at depth is on average 1.6 times larger than at the surface [*Villamor and Berryman*, 2001]. A correction factor of 1.6 applied to the surface dip slip across the Whakatane Graben results in a dip-slip rate of 13.7 ± 3.1 mm yr^{-1} at seismogenic depth (Table 2). This rate is independent of the fault dip at crustal depth. From crustal dip-slip rate, an extension rate is calculated using a fault dip of 45° ± 15°. An additional correction factor of 1.3 is then applied to account for the contribution to extension of small earthquakes that do not rupture the surface. We thus calculate a crustal extension rate of 12.6 ± 5.7 mm yr^{-1} in the offshore Whakatane Graben (Table 2).

8.3. Regional Implications

[54] Dextral shear in the North Island diminishes from ~20 mm yr^{-1} at Wellington (Figure 1 insert) to not more than a few millimeters at the Bay of Plenty [*Beanland*, 1995; *Beanland and Haines*, 1998]. *Mouslopoulou et al.* [2004] interpreted that the northward decrease in strike-slip displacement on the NIDFB within 100 km of the Bay of Plenty is accompanied by an increase in dip-slip displacement along the faults, and could contribute to the total back-arc extension where the NIDFB intersects the Whakatane graben from the coast of the Bay of Plenty, northward.

[55] We recalculate an extension rate of 7.8 ± 3.5 mm yr^{-1} in the TFB, 50 to 80 km south of the coast of the Bay of Plenty, using the surface throw rate of 7.2 mm yr^{-1} from *Villamor and Berryman* [2001], but incorporating the contribution of antithetic faults, and using their preferred fault dips of 75° and 60° for surface and crustal depth, respectively (Table 2). This rate is 4.8 mm yr^{-1} lower than our extension rate of 12.6 mm yr^{-1} in the Whakatane Graben where fault dips are constrained by focal mechanisms and seismic reflection data. *Villamor and Berryman* [2001] and *Acocella et al.* [2003] argue that fault dips are steeper in the onshore TFB, south of the Okataina Volcanic Center, on the basis of little evidence for significant domino rotation, immaturity of the rifting processes, and considering Andersonian theory of fault mechanics whereby pure extensional stress across the rift enhances high-angle faulting. We recognize that there are structural and kinematic differences between the Whakatane Graben and the TFB south of the Okataina Volcanic Centre, which may be reflected in the dip of the faults at crustal depth, but consider that additional constraints on fault geometry south of the Okataina Volcanic Centre are required. Should the fault geometry prove to be comparable in both areas (i.e., 70° at the surface, 45° at seismogenic depths), the resulting extension rate would be 11.3 ± 5.1 mm yr^{-1} in the TFB.

[56] These data indicate that extension rates along the Taupo rift system increase northward across the Okataina Volcanic Centre (OVC), by a minimum of 1.3 to up to 4.8 mm yr^{-1}. The upper range of 4.8 mm yr^{-1} is associated with the uncertainty on the dip of the seismogenic faults on both sides of the OVC. This increase compares favorably with a northward increase of about 6 mm yr^{-1} (9.6 to 15.6 mm yr^{-1}) over the same length of the rift, modeled by *Wallace et al.* [2004]. We believe, therefore that the minimum difference of 1.3 mm yr^{-1} between extension rates on either sides of the OVC, as calculated in this study, is meaningful, as it corresponds to the case where both parts of the rift have similar high fault dips. In all cases, the OVC acts as a large-scale transfer zone between the TFB and the Whakatane Graben, as already inferred by *Rowland and Sibson* [2001] and *Acocella et al.* [2003]. The most significant difference in the tectonic settings north of the OVC compared with the south is the junction of the NIDFB with the rift. Hence we argue that the increase in extension rate in the Whakatane Graben compared with that in the TFB, is

in part due to the contribution of the NIDFB as it intersects the rift, a conclusion that validates the prediction of *Mouslopoulos et al.* [2004].

[57] In this study, we estimated an average rifting direction of about N330°E from a variety of sources (section 8.1), at about 20° oblique to the orthogonal extensional direction (Figure 15). This implies a dextral component of up to 4.6 ± 2.1 mm yr^{-1} (36%, Table 2) occurs parallel to the rift axis. The similar orientations of the faults in the graben center and the Edgecumbe Fault, as well as the focal mechanisms of the 1987 Edgecumbe and 1992 Bay of Plenty earthquakes (Figure 4 and Table 3) indicate that these faults fail in pure dip-slip displacement events, in the direction of the rifting. Because of the large contribution of these faults to the extension (~50%) (Table 1), we infer that more than 50% of the rift axis-parallel motion, i.e., ~2.5 mm yr^{-1}, may be accommodated on these pure dip-slip faults. Observations along the Matata Fault [*Acocella et al.*, 2003] together with the Matata earthquake swarm mechanisms [*Richardson*, 1989], indicate that faults along the margins of the graben, parallel to the rift axis, are more likely to rupture in oblique slip displacement events (Figure 15). Hence we conclude that the dextral component of oblique rifting is probably distributed between dip-slip faults in the center and oblique slip structures on the border of the graben.

9. Conclusions

[58] Oblique rifting over the continental shelf of the Bay of Plenty is characterized by widespread faulting extending across the 20-km-wide Whakatane Graben. Multichannel and high-resolution seismic reflection data provide a pseudo-three-dimensional image of the active structures. The pervasive post last glacial transgressive surface beneath the continental shelf of the Bay of Plenty provides an excellent, albeit diachronous, marker. The age of this horizon is determined to range from 7.5 to 20.5 ka, by correlating its depth beneath sea level to a recalibrated global sea level curve, and by taking into account estimates of regional subsidence in the center of the graben and uplift on its margins.

[59] The active rift system trends N43°E and includes 15 major fault zones. The eastern boundary of the graben is represented by the NW dipping White Island Fault, with a maximum surface dip-slip rate of up to 2.3–3.5 mm yr^{-1}. Strain concentrates in the central and eastern part of the graben, where the dip-slip rate for the last 17 kyr reaches up to 3.7 mm yr^{-1} on individual fault zones. To the west of the graben axis, faulting is distributed across six fault zones located over the uplifted Rurima Ridge, with dip slip on individual structures ranging 1.4 to 2.6 mm yr^{-1}. The western margin corresponds to the Tarawera Fault, which displaces basement by more than 2 km, but has a low (<0.5 mm yr^{-1}) recent displacement rate. The decrease of finite strain along the western border of the graben contrasts with the present-day high strain in its central and eastern parts, which is consistent with the hypothesis of *Davey et al.* [1995] that deformation is migrating to the east.

[60] Cumulative surface dip-slip rate across the 20-km-wide Whakatane Graben reaches 8.5 ± 1.9 mm yr^{-1}. The surface dip-slip rate is utilized to estimate a crustal extension rate of 12.6 ± 3.5 mm yr^{-1} across the graben, using a seismogenic fault dip of 45° ± 15° and applying correction factors determined by *Villamor and Berryman* [2001] for crustal deformation. The rift obliquity of ~20° deduced from earthquake focal mechanisms, geodetic extension azimuths, and field data is consistent with the fault geometry in the graben. The obliquity yields a 13.4 mm yr^{-1} rifting rate along a N331°E direction, and up to 4.6 mm yr^{-1} of parallel to the axis. About half of the rift parallel motion is accommodated by pure dip-slip displacement on central faults trending oblique to the rift axis, while half accrues in oblique-slip faults near the margins.

[61] **Acknowledgments.** We used Globe Claritas® (GNS Science, Lower Hutt, New Zealand) to process NIWA multichannel seismic data. This manuscript benefited from discussions with Susanna Taylor (now at University College, Dublin) and Huw Horgan (now at Penn State University). We thank Pilar Villamor (GNS Science) for an early review of the manuscript, Miles Dunkin (NIWA, Wellington) for digitizing all structural interpretations, and Brett Grant (NIWA) for assisting with figure graphics. Mike Stevens, Wanda Stratford (Victoria University of Wellington), and Huw Horgan processed part of the multichannel seismic data. Fred Davey and Stuart Henrys (GNS Science) are thanked for access to the Explora seismic line. This work was funded by the New Zealand Foundation for Research Science and Technology (contract CO1X0203) and the Natural Environment Research Council (GR3/11862).

References

Acocella, V., K. Spinks, J. Cole, and A. Nicol (2003), Oblique back arc rifting of Taupo Volcanic Zone, New Zealand, *Tectonics*, *22*(4), 1045, doi:10.1029/2002TC001447.

Adams, D. A. (1983), Some methods of analysis of geodetic data and their applications to the measurements of crustal deformation, M.Sc. thesis, 101 pp., Victoria Univ., Wellington, New Zealand.

Anderson, H., and T. Webb (1989), The rupture process of the Edgecumbe earthquake, New Zealand, *N. Z. J. Geol. Geophys.*, *32*, 43–52.

Anderson, H., E. Smith, and R. Robinson (1990), Normal faulting in a back-arc basin: Seismological characteristics of the March 2, 1987, Edgecumbe, New Zealand, Earthquake, *J. Geophys. Res.*, *95*(B4), 4709–4723.

Beanland, S. (1995), The North Island Dextral Fault Belt, Hikurangi subduction margin, New Zealand, Ph.D. thesis, 341 pp., Victoria Univ. of Wellington, Wellington, New Zealand.

Beanland, S., and J. Haines (1998), The kinematics of active deformation in the North Island, New Zealand, determined from geological strain rates, *N. Z. J. Geol. Geophys.*, *41*, 311–323.

Beanland, S., K. R. Berryman, and G. H. Blick (1989), Geological investigations of the 1987 Edgecumbe earthquake, New Zealand, *N. Z. J. Geol. Geophys.*, *32*, 73–91.

Beanland, S., G. H. Blick, and D. J. Darby (1995), Normal faulting in a back-arc basin: Geological and geodetic characteristics of the 1987 Edgecumbe, earthquake, New Zealand, *J. Geophys. Res.*, *95*(B4), 4693–4708.

Bibby, H. M., T. G. Caldwell, F. J. Davey, and T. H. Webb (1995), Geophysical evidence on the structure of the Taupo Volcanic Zone and its hydrothermal circulation, *J. Volcanol. Geotherm. Res.*, *68*(1–3), 29–58.

Bryan, C. J., S. Sherburn, H. M. Bibby, S. C. Bannister, and A. W. Hurst (1999), Shallow seismicity of the central Taupo Volcanic Zone, New Zealand: Its distribution and nature, *N. Z. J. Geol. Geophys.*, *42*, 533–542.

Bull, J. M., P. M. Barnes, G. Lamarche, D. J. Sanderson, P. A. Cowie, S. K. Taylor, and J. K. Dix (2006), High-resolution record of displacement accumulation on an active normal fault: Implications for models of slip accumulation during repeated earthquakes, *J. Struct. Geol.*, doi:10.1016/j.jsg.2006.03.006, in press.

Carter, R. M., L. Carter, and D. P. Johnson (1986), Submergent shorelines in the south-west Pacific: Evidence for an episodic post-glacial transgression, *Sedimentology*, *33*, 629–649.

Chapman, T. J., and A. W. Meneilly (1991), The displacement patterns associated with a reverse-reactivated, normal growth fault, in *The Geometry of Normal Faults*, edited by A. M. Roberts, G. Yielding and B. Freeman, *Geol. Soc. Spec. Publ.*, *56*, 183–191.

Clifton, A. E., R. W. Schlische, M. O. Withjack, and R. V. Ackermann (2000), Influence of rift obliquity on fault-population systematics: Results of experimental clay models, *J. Struct. Geol.*, *22*, 1491–1509.

Crook, C. N., and J. Hannah (1989), Regional horizontal deformation associated with the 1987 Edgecumbe earthquake, Bay of Plenty, New Zealand: An introduction, *N. Z. J. Geol. Geophys.*, *32*, 93–98.

Darby, D. J. (1989), Dislocation modelling of the 1987 Edgecumbe earthquake, New Zealand, *N. Z. J. Geol. Geophys.*, *32*, 115–122.

Darby, D. J., K. M. Hodgkinson, and G. H. Buck (2000), Geodetic measurement of deformation in the Taupo Volcanic Zone, New Zealand: The north Taupo network revisited, *N. Z. J. Geol. Geophys.*, *43*, 157–170.

Davey, F. J., S. A. Henrys, and E. Lodolo (1995), Asymmetric rifting in a continental back-arc environment, North Island, New Zealand, *J. Volcanol. Geoth. Res.*, *68*(1/3), 209–238.

DeMets, C., R. G. Gordon, D. F. Argus, and S. Stein (1994), Effect of recent revisions to the geomagnetic reversal time scale on estimates of current plate motions, *Geophys. Res. Lett.*, *21*(20), 2191–2194.

Gibbs, A. D. (1990), Linked fault families in basin formation, *J. Struct. Geol.*, *12*, 795–803.

Grasemann, B., S. Martel, and C. Passchier (2005), Reverse and normal drag along a fault, *J. Struct. Geol.*, *27*, 999–1010, doi:10.1016/j.jsg.2005.04.006.

Harrison, A. J., and R. S. White (2004), Crustal structure of the Taupo Volcanic Zone, New Zealand: Stretching and igneous intrusion, *Geophys. Res. Lett.*, *31*, L13615, doi:10.1029/2004GL019885.

Herzer, R. H. (1981), Late Quaternary stratigraphy and sedimentation of the Canterbury continental shelf, New Zealand, *N. Z. Oceanogr. Inst. Mem.*, *89*, 71 pp.

Horgan, H. J. (2003), The thermal and crustal structure of a continental back-arc basin: Offshore Bay of Plenty, New Zealand, M.Sc. thesis, 141 pp., Victoria Univ. of Wellington, Wellington, New Zealand.

Houghton, B. F., C. J. N. Wilson, M. O. McWilliams, M. A. Lanphere, S. D. Weaver, R. M. Briggs, and M. S. Pringle (1995), Chronology and dynamics of a large silicic magmatic system: Central Taupo Volcanic Zone, New Zealand, *Geology*, *23*, 13–16.

Jackson, J., and D. McKenzie (1983), The geometrical evolution of normal fault system, *J. Struct. Geol.*, *5*, 471–482.

Jackson, J. A. (1987), Active normal faulting and crustal extension, in *Continental Extensional Tectonics*, edited by M. P. Coward, J. F. Dewey, and P. L. Hancock, *Geol. Soc. Spec. Publ.*, *28*, 3–17.

Jackson, J. A., and N. J. White (1989), Normal faulting in the upper continental crust: Observations from regions of active extension, *J. Struct. Geol.*, *11*, 15–36.

Kohn, B. P., and G. P. Glasby (1978), Tephra distribution and sedimentation rates in the Bay of Plenty, New Zealand, *N. Z. J. Geol. Geophys.*, *21*, 49–70.

Kronberg, P. (1991), Geometries of extensional fault systems, observed and mapped on aerial and satellite photographs of Central Afar (Ethiopia/Djibouti), *Geol. Mijnbouw*, *70*, 145–161.

Lamarche, G., J. M. Bull, P. M. Barnes, S. K. Taylor, and H. J. Horgan (2000), Constraining fault growth rates and fault evolution in the Bay of Plenty, New Zealand, *Eos Trans. AGU*, *81*(42), 481, 485–486.

Lewis, K. B., and H. M. Pantin (1984), Intersection of a marginal basin with a continent: Structure and sediments of the Bay of Plenty, New Zealand, in *Marginal Basin Geology*, edited by B. P. Kokelaar and M. F. Howells, *Geol Soc. Spec. Publ.*, *6*, 121–135.

Mansfield, C. S., and J. A. Cartwright (1996), High resolution fault displacement mapping from three-dimensional seismic data: Evidence for dip linkage during fault growth, *J. Struct. Geol.*, *18*, 249–263.

McClay, K. R. (1996), Recent advances in analogue modelling: Uses in section construction and validation, in *Modern Developments in Structural Interpretation, Validation and Modelling*, edited by P. G. Buchanan and D. A. Nieuwland, *Geol. Soc. Spec. Publ.*, *99*, 201–225.

McClay, K. R., and S. Khalil (1998), Extensional hard linkages, eastern Gulf of Suez, Egypt, *Geology*, *26*, 563–566.

McClay, K. R., and M. J. White (1995), Analogue modelling of orthogonal and oblique rifting, *Mar. Pet. Geol.*, *12*, 137–151.

Morley, C. K., W. A. Wescott, D. M. Stone, R. M. Harper, S. T. Wigger, and F. M. Karanja (1992), Tectonic evolution of the northern Kenyan Rift, *J. Geol. Soc. London*, *149*, 333–348.

Mouslopoulou, V., A. Nicol, T. A. Little, K. R. Berryman, and J. J. Walsh (2004), Fault interactions and slip transfer between the North Island dextral fault belt and the Taupo rift, New Zealand, in *Programme and Abstracts, Geological Society of New Zealand/New Zealand Geophysical Society/26th Annual Geothermal Workshop Combined Conference "Geo3", Taupo, New Zealand, Misc. Publ. 117A*, edited by V. Manville and D. Tilyard, p. 71, Geol. Soc. of N. Z., Lower Hutt.

Nairn, I. A., and S. Beanland (1989), Geological setting of the 1987 Edgecumbe earthquake, New Zealand, *N. Z. J. Geol. Geophys.*, *32*, 1–14.

Richard, P. (1991), Experiments on faulting in a two-layered cover sequence overlying a reactivated basement fault with oblique-slip, *J. Struct. Geol.*, *13*, 459–469.

Richardson, W. P. (1989), The Matata earthquake of 1977 May 31: A recent event near Edgecumbe, Bay of Plenty, New Zealand, *N. Z. J. Geol. Geophys.*, *32*, 17–30.

Roberts, G. P., P. A. Cowie, I. Papanikolaou, and A. M. Michetti (2004), Fault scaling relationships, deformation rates and seismic hazards: An example from the Lazio-Abruzzo Apennines, central Italy, *J. Struct. Geol.*, *26*, 377–398.

Rowland, J. V., and R. H. Sibson (2001), Extensional fault kinematics within the Taupo Volcanic Zone, New Zealand: Soft-linked segmentation of a continental rift system, *N. Z. J. Geol. Geophys.*, *44*, 271–283.

Scott, D. L., M. A. Etheridge, and B. R. Rosendahl (1992), Oblique-slip deformation in extensional terrains: A case study of the lakes Tanganyika and Malawi rift zones, *Tectonics*, *11*, 998–1009.

Sissons, B. A. (1979), The horizontal kinematics of the North Island of New Zealand, Ph.D. thesis, 117 pp., Victoria Univ., Wellington.

Stern, T. A. (1985), A back-arc basin formed within continental lithosphere: The central volcanic region of New Zealand, *Tectonophysics*, *112*, 385–409.

Stratford, W. R., and T. A. Stern (2004), Strong seismic reflections and melts in the mantle of a continental back-arc basin, *Geophys. Res. Lett.*, *31*, L06622, doi:10.1029/2003GL019232.

Stuiver, M., P. J. Reimer, E. Bard, J. W. Beck, G. S. Burr, K. A. Hughen, B. Kromer, G. McCormac, J. van der Plicht, and M. Spurk (1998), INTCAL98 radiocarbon age calibration, 24,000–0 cal BP, *Radiocarbon*, *3*, 1041–1083.

Taylor, S. K. (2003), A long timescale high-resolution fault activity history of the Whakatane Graben, Bay of Plenty, New Zealand, Ph.D. thesis, 210 pp., Univ. of Southampton, Southampton, U. K..

Taylor, S. K., J. M. Bull, G. Lamarche, and P. M. Barnes (2004), Normal fault growth and linkage in the Whakatane Graben, New Zealand during the last 1.3 Myr, *J. Geophys. Res.*, *109*, B02408, doi:10.1029/2003JB002412.

Tron, V., and J. P. Brun (1991), Experiments on oblique rifting in brittle ductile systems, *Tectonophysics*, *188*, 71–84.

Villamor, P., and K. R. Berryman (2001), A late Quaternary extension rate in the Taupo Volcanic Zone, New Zealand, derived from fault slip data, *N. Z. J. Geol. Geophys.*, *44*, 243–269.

Walcott, R. I. (1984), Reconstruction of the New Zealand region for the Neogene, *Paleogeogr. Paleoclimatol. Paleoecol.*, *46*, 217–231.

Walcott, R. I. (1987), Geodetic strain and the deformation history of the North Island of New Zealand during the late Cainozoic, *Philos. Trans. R. Soc. London, Ser. A*, *321*, 163–181.

Wallace, L. M., J. Beavan, R. McCaffrey, and D. Darby (2004), Subduction zone coupling and tectonic block rotations in the North Island, New Zealand, *J. Geophys. Res.*, *109*, B12406, doi:10.1029/2004JB003241.

Webb, T. H., and H. J. Anderson (1998), Focal mechanisms of large earthquakes in the North Island of New Zealand: Slip partitioning at an oblique active margin, *Geophys. J. Int.*, *134*, 40–86.

Wells, D. L., and K. J. Coppersmith (1994), New empirical relationships among magnitude, rupture length, rupture width, rupture area, and surface displacement, *Bull. Seismol. Soc. Am.*, *84*(4), 974–1002.

Wilson, C. J. N., B. F. Houghton, M. O. McWilliams, M. A. Lanphere, S. D. Weaver, and R. M. Briggs (1995), Volcanic and structural evolution of the Taupo Volcanic Zone, New Zealand: A review, *J. Volcanol. Geotherm. Res.*, *68*, 1–28.

Withjack, M. O., J. Olson, and E. Peterson (1990), Experimental models of extensional forced folds, *AAPB Bull.*, *74*, 1038–1054.

Woodward, D. J. (1989), Geological structure of the Rangitaiki plain near Edgecumbe, New Zealand, from seismic data, *N. Z. J. Geol. Geophys.*, *32*, 15–16.

Wright, I. C. (1990), Late Quaternary faulting of the offshore Whakatane Graben, Taupo Volcanic Zone, New Zealand, *N. Z. J. Geol. Geophys.*, *33*, 245–256.

Wright, I. C. (1992), Shallow structure and active tectonism of an offshore continental back-arc spreading system: The Taupo Volcanic Zone, New Zealand, *Mar. Geol.*, *103*, 287–309.

P. M. Barnes and G. Lamarche, National Institute of Water and Atmospheric Research (NIWA) Ltd, Private bag 14-901, Wellington, New Zealand. (g.lamarche@niwa.co.nz)

J. M. Bull, National Oceanography Centre Southampton, University of Southampton, Southampton SO14 3 ZH, UK.